Identification of a dTDP-rhamnose biosynthetic pathway that oscillates with the molting cycle in *Caenorhabditis elegans*

Likui Feng*, Qingyao Shou* and Rebecca A. Butcher*[1]

*Department of Chemistry, University of Florida, Gainesville, FL 32611, U.S.A.

L-Rhamnose is a common component of cell-wall polysaccharides, glycoproteins and some natural products in bacteria and plants, but is rare in fungi and animals. In the present study, we identify and characterize a biosynthetic pathway for dTDP-rhamnose in *Caenorhabditis elegans* that is highly conserved across nematode species. We show that RML-1 activates glucose 1-phosphate (Glc-1-P) in the presence of either dTTP or UTP to yield dTDP-glucose or UDP-glucose, respectively. RML-2 is a dTDP-glucose 4,6-dehydratase, converting dTDP-glucose into dTDP-4-keto-6-deoxyglucose. Using mass spectrometry and NMR spectroscopy, we demonstrate that coincubation of dTDP-4-keto-6-deoxyglucose with RML-3 (3,5-epimerase) and RML-4 (4-keto-reductase) produces dTDP-rhamnose. RML-4 could only be expressed and purified in an active form through co-expression with a co-regulated protein, RML-5, which forms a complex with RML-4. Analysis of the sugar nucleotide pool in *C. elegans* established the presence of dTDP-rhamnose *in vivo*. Targeting the expression of the rhamnose biosynthetic genes by RNAi resulted in significant reductions in dTDP-rhamnose, but had no effect on the biosynthesis of a closely related sugar, ascarylose, found in the ascaroside pheromones. Therefore, the rhamnose and ascarylose biosynthetic pathways are distinct. We also show that transcriptional reporters for the rhamnose biosynthetic genes are expressed highly in the embryo, in the hypodermis during molting cycles and in the hypodermal seam cells specifically before the molt to the stress-resistant dauer larval stage. These expression patterns suggest that rhamnose biosynthesis may play an important role in hypodermal development or the production of the cuticle or surface coat during molting.

Key words: biosynthesis, *Caenorhabditis elegans*, dTDP-glucose 4,6-dehydratase, hypodermis, molting, rhamnose.

INTRODUCTION

The 3-deoxysugar L-rhamnose is commonly found in polysaccharide and glycoprotein components of the cell wall of bacteria and plants, as well as in various natural products, but is rarely found in fungi and animals [1]. In bacteria, L-rhamnose is a constituent of several types of O-antigens, which often are covalently linked to lipopolysaccharides in the outer leaflet of the outer cell membrane. These O-antigens are associated with bacterial virulence and facilitate bacterial evasion of immune system defences [2]. In plants, L-rhamnose is a key sugar found in rhamnogalacturanan I and II, which are primary constituents of the pectins, complex polysaccharides in the plant cell wall [3,4]. L-Rhamnose is also often found in some O-linked glycoproteins in the plant cell wall that influence growth, morphogenesis and responses to various stresses [5]. L-Rhamnose is also part of many natural plant compounds, including flavonoids, terpenoids and saponins. Recently, L-rhamnose was found to be a component of a phosphoglycan from trypanosomes [6].

In bacteria and plants, the biosynthesis of UDP/dTDP-rhamnose from glucose 1-phosphate (Glc-1-P) is well characterized and is usually accomplished in a few steps: the formation of UDP/dTDP-glucose, followed by a 4,6-dehydration to produce UDP/dTDP-4-keto-6-deoxyglucose, followed by 3,5-epimerization and 4-keto-reduction to form UDP/dTDP-rhamnose [1,7–9]. In *Escherichia coli*, the pathway converts dTDP-glucose (dTDP-Glc) into dTDP-rhamnose, and the four steps in the pathway are catalyzed by four separate enzymes (RmlA–RmlD) [10–16]. Conversely, in plants, the pathway converts UDP-glucose (UDP-Glc) into UDP-rhamnose, and the last three steps in the pathway are catalyzed by a single polypeptide, encoded by the RHM gene family, with dehydratase, epimerase and reductase activities [17].

In *Caenorhabditis elegans* and other nematodes, O- and N-linked glycoproteins and glycolipids have been shown to play important roles in embryonic and larval development and in mediating interactions with pathogens [18]. The outer surface of *C. elegans* is covered by a protective cuticle, which is secreted by an underlying layer of epithelial cells, including the hypodermis and seam cells [19]. Glycoproteins are present in the cuticle matrix and are also secreted, coating the outer surface of the cuticle. Glycolipids are also present in this surface coat. After hatching from an egg, *C. elegans* proceeds through four larval stages (L1–L4) to the adult, but will enter a stress-resistant alternative L3 larval stage (the 'dauer' stage) under conditions of high population density and low food [20]. At each larval stage during development, a new stage-specific cuticle is made, resulting in changes in surface coat glycoproteins and glycolipids. Mutations that interfere with the production of glycoproteins and glycolipids in *C. elegans* are associated, for example, with abnormal surface epitope expression (Srf, *s*ur*f*ace antigenicity abnormal phenotype) and pathogen resistance (Bus, *b*acterially *uns*wollen) [21,22]. To our knowledge, rhamnose has not been detected in the *C. elegans* cuticle. It has been claimed that a single

Abbreviations: ADP, adenosine 5′-diphosphate; CDP, cytosine 5′-diphosphate; dTDP, 2′-deoxythymidine 5′-diphosphate; dTDP-Glc, dTDP-glucose; GDP, guanosine 5′-diphosphate; GDP-Fuc, GDP-fucose; GDP-Man, GDP-mannose; Glc-1-P, glucose 1-phosphate; IPTG, isopropyl β-D-1-thiogalactopyranoside; Man-1-P, mannose 1-phosphate; MCS, multiple cloning site; MESG, 2-amino-6-mercapto-7-methylpurine ribonucleoside; NGM, nematode growth medium; RBL, rhamnose-binding lectin; SDR, short-chain dehydrogenase/reductase; SIM, selected ion monitoring; TEAA, triethylammonium acetate; UDP-Gal, UDP-galactose; UDP-Glc, UDP-glucose; UDP-GlcNAc, UDP-*N*-acetyl-glucosamine.

[1] To whom correspondence should be addressed (email butcher@chem.ufl.edu).

glycoprotein extracted from the surface of the parasitic nematode *Ascaridia galli* contained rhamnose [23]. However, direct mass spectrometric proof of rhamnose in a nematode macromolecule is yet to be published.

During embryonic and larval development in *C. elegans*, glycoproteins have been shown to be critical for cell migration and patterning. For example, the latrophilin receptor homolog *lat-1* is essential for the establishment of tissue polarity and the alignment of cell division planes in the developing *C. elegans* embryo [24]. Latrophilin receptors all contain a highly conserved RBL (rhamnose-binding lectin) domain. The *lat-1* RBL domain plays an essential role, since rescue of the embryonic lethality of *lat-1* mutant with a *lat-1* transgene requires the presence of the RBL domain in the transgene. However, it has been reported that rhamnose-binding activity for the *lat-1* RBL domain could not be detected [24]. Thus, it is unclear whether this domain binds to specific carbohydrates of glycoproteins and whether this binding is necessary for the *lat-1* receptor to mediate cell–cell interactions.

Although our analysis has shown that homologs of bacterial and plant rhamnose biosynthetic genes are present in most nematode species, rhamnose biosynthesis has not been studied in nematodes. In the present study, we demonstrate the *in vitro* activity of rhamnose biosynthetic genes from *C. elegans* and show that these genes are required for dTDP-rhamnose biosynthesis *in vivo*. RML-1 is a UTP/dTTP-glucose-1-phosphate uridylyl/thymidylyl transferase, RML-2 is a dTDP-glucose 4,6-dehydratase, RML-3 is a 3,5-epimerase, RML-4 is a 4-keto-reductase and RML-5 is an RML-4-associated protein that is necessary for RML-4 expression and/or activity. We show that transcriptional reporters for the rhamnose biosynthetic genes are expressed in the embryo, in the hypodermis during larval molting cycles, and in the hypodermal seam cells, specifically in recovered L1 larvae and in pre-dauers. These expression patterns suggest that rhamnose biosynthesis may play a role in molting or the production of the cuticle or surface coat at specific molts. Rhamnose is not thought to be made by humans, since neither rhamnose nor the rhamnose biosynthetic pathway has been found in humans. Thus, given that RML-4 and RML-5 are essential for embryonic and larval development and do not have close human homologs, they could potentially be investigated as targets for novel anthelmintics.

EXPERIMENTAL

Phylogenetic tree analysis

The protein sequences of RML-1–5 and its homologs in both free-living and parasitic nematode species were retrieved from Wormbase. MEGA6.0 was used to generate the neighbor-joining tree [25].

RNAi

RNAi was carried out by feeding bacteria expressing double-stranded RNA as described in [26] with modifications. Briefly, nematode growth medium (NGM) agar plates with 25 mg/l carbenicillin and 1 mM isopropyl β-D-1-thiogalactopyranoside (IPTG) in 6 cm dishes were prepared and left at room temperature for 4–7 days before use. Bacteria carrying appropriate RNAi clones were grown in 5 ml of LB containing 150 mg/l ampicillin at 225 rev./min, 37 °C, for 6–10 h, and 200 μl of bacterial culture was transferred to each plate. The plates were left at room temperature overnight to let the bacterial lawn dry. Twenty L4 *rrf-3* worms were moved on to each plate, allowed to lay eggs for 24 h and then removed. Worms were cultivated at 20 °C for 3 days, and phenotypes were examined.

Construction of plasmids for protein expression

All genes were amplified by PCR using Pfu polymerase (New England Biolabs) from a *C. elegans* cDNA library. *gmp-1* (C42C1.5), *ugp-1* (D1005.2), *rml-1* (K08E3.5), *rml-2* (F53B1.4) and *rml-3* (C14F11.6) genes were inserted into the pET-30a vector separately such that they could be expressed with an N-terminal His tag. For co-expression of RML-4 (C01F1.3) and RML-5 (Y71G12B.6), *rml-4* was inserted into multiple cloning site (MCS) 1 of pACYC-Duet1 with an N-terminal His tag, and *rml-5* was inserted into MCS2 of pACYC-Duet1 without any tag. All primers used in the present study are listed and restriction sites underlined in Supplementary Table S1. All gene sequences were confirmed by sequencing. Constructed plasmids containing *gmp-1*, *ugp-1*, *rml-1*, *rml-2*, *rml-3* or *rml-4*/*rml-5* were transformed into *E. coli* BL21(DE3) cells (New England Biolabs) independently for expression. *rml-5* (N-terminal His tag) in pET-28a and *rml-4* (no tag) in MCS2 of pACYC-Duet1 or *rml-4* (N-terminal His tag) in pET-28a and *rml-5* (no tag) in MCS2 of pACYC-Duet1, were also co-transformed into BL21(DE3) cells.

Protein expression and purification

Cells transformed with pET-30a-*gmp-1*, *ugp-1*, *rml-1*, *rml-2* or *rml-3* were grown in LB broth under appropriate antibiotic selection at 37 °C to D_{600} 0.6–0.8, protein expression was induced with 0.2 mM IPTG, and cells were grown at 20 °C for 20 h. For co-expression of *rml-4* and *rml-5*, cells transformed with pACYC-Duet1-rml-4/rml-5 or co-transformed with two plasmids were grown in LB broth under appropriate antibiotic selection, protein expression was induced with 0.1 mM IPTG, and cells were grown at 16 °C for 20 h. All purification steps were carried out at 4 °C. Briefly, cells were collected by centrifugation at 6084 ***g*** for 10 min, and resuspended in lysis buffer (20 mM Tris/HCl and 500 mM NaCl, pH 7.5). The cells were then lysed by microfluidizer three times and centrifuged at 38 828 ***g*** for 20 min. The supernatant was incubated with 1 ml of pre-equilibrated nickel resin (Thermo Scientific) for 1 h by shaking on ice. The resin was washed with 15 ml of lysis buffer, 15 ml of washing buffer (20 mM Tris/HCl, 500 mM NaCl and 20 mM imidazole, pH 7.5) and eluted with buffer containing 250 mM imidazole. The eluted sample was concentrated and loaded on to an FPLC column connected to a Superdex 200 gel-filtration column (GE Healthcare) with buffer (20 mM Tris/HCl and 100 mM NaCl, pH 7.5). Protein concentration was determined by using Quick Start™ Dye reagent (Bio-Rad Laboratories) with 2 mg/ml bovine serum albumin used as a standard. Purified proteins were flash-frozen in 10 % glycerol and stored at − 80 °C.

Pyrophosphorylase activity assay and kinetic studies

The pyrophosphorylase activities of GMP-1, UGP-1 and RML-1 were measured using a spectrophotometric pyrophosphate assay, according to the manufacturer's method for the EnzChek pyrophosphate assay kit (Invitrogen). The standard reaction (100 μl total volume) contained 0.25 mM 2-amino-6-mercapto-7-methylpurine ribonucleoside (MESG) (Santa Cruz Biotechnology), 1 mM sugar 1-phosphate [Glc-1-P or Man-1-P (mannose 1-phosphate)], 1 mM NTP (ATP, GTP, CTP, dTTP or UTP), 0.1 unit of purine nucleoside phosphorylase and 0.04 unit of inorganic pyrophosphorylase in 50 mM Tris/HCl, 5 mM $MgCl_2$

and 1 mM DTT, pH 7.5. Reactions were pre-incubated for at least 10 min to remove the background phosphate and initiated by adding 2 μM purified enzyme. Reactions were carried out at 25 °C and monitored using the absorbance at 360 nm on an Agilent 8453 UV/VIS spectrophotometer. The initial rate (AU/s) was measured over the first 5 min. To confirm the formation of a particular NDP-sugar during reactions, LC–MS was used to detect the relevant ion (ADP-Glc, *m*/*z* 588; dTDP-Glc, *m*/*z* 563; GDP-Glc, *m*/*z* 604; CDP-Glc, *m*/*z* 564; UDP-Glc, *m*/*z* 565; GDP-Man, *m*/*z* 604). For kinetics, reactions contained 1 mM sugar 1-phosphate (Glc-1-P or Man-1-P) with various concentrations of NTP (GTP, dTTP or UTP) or 1 mM NTP (GTP, dTTP or UTP) with various concentrations of sugar 1-phosphate (Glc-1-P or Man-1-P), as well as 0.25 mM MESG, 0.1 unit of purine nucleoside phosphorylase, 0.04 unit of inorganic pyrophosphorylase (in 50 mM Tris/HCl, 5 mM $MgCl_2$ and 1 mM DTT, pH 7.5) and 4–5 μg of recombinant enzyme. The concentration of the product pyrophosphate was calculated based on a calibration curve made using pyrophosphate (Invitrogen) as a standard. K_m and k_{cat} were calculated by fitting each data set to the Michaelis–Menten algorithm in GraphPad Prism software, and the S.D. of k_{cat}/K_m was calculated using the Fenner formula [27].

Dehydratase activity assay

Dehydratase activity was measured by detecting the product NDP-4-keto-6-deoxyglucose, which has a characteristic absorbance at 320 nm under alkaline conditions [28]. First, all substrate NDP-sugars were generated by the pyrophosphorylase reaction, the reaction mixtures were divided into aliquots, and NAD^+ (0.5 mM) was added. Then, reactions were initiated by adding RML-2 (2 μM final concentration) and incubating at 25 °C for 60 min. Heat-treated samples were cooled on ice and centrifuged for 10 min at 15 871 ***g***. The supernatant was made alkaline (0.1 M sodium hydroxide final concentration in 100 μl total volume) and incubated at 37 °C for 20 min before measuring absorbance. Negative controls were carried out in the absence of enzyme.

Reductase activity assay

The substrate dTDP-4-keto-6-deoxyglucose was produced through the overnight reaction of RML-2 (2 μM) with dTDP-Glc (1 mM) and NAD^+ (0.5 mM) and the reaction mixture was then incubated with RML-3 and/or RML-4–RML-5 (2 μM) in the presence of NAD(P)H (1 mM). Negative controls were performed without RML-2 or NAD(P)H. Substrate UDP-Glc (1 mM) was incubated with RML-2 and/or RML-3 and/or RML-4–RML-5 (2 μM) in the presence of NAD^+ (0.5 mM) and NAD(P)H (1 mM). A negative control was performed without any enzymes or NAD(P)H. Reactions were carried out at 25 °C for 30 min, monitoring the absorbance at 370 nm, which indicated the consumption of NAD(P)H [29,30].

Sequence alignment, structural modeling and superposition

Amino acid sequence alignment of RML-3 with *E. coli* RmlC (GenBank accession number AFC91454) was completed by using ClustalW. Modeling of the RML-4 structure was achieved via Robetta [31]. *Streptococcus suis* RmlB without substrate bound (PDB code 1OC2) and *Ec*RmlD (PDB code 1KBZ) were used as the templates for RML-4 N-terminal (amino acids 1–344) and C-terminal domain (amino acids 345–631) modeling. Superposition of the RML-4 structure model with dTDP-Glc-bound *Ss*RmlB (PDB code 1KER) was done using PyMol (http://www.pymol.org).

Mass spectrometry of reaction products

Products of all reactions were analyzed by LC–MS using a Luna 5 μm C_{18} (2) column (100 mm × 4.6 mm; Phenomenex) coupled to an Agilent 6130 single quad mass spectrometer operating in negative scan mode. A solvent gradient was used: 95 % buffer A, 5 % buffer B, 0 min; 80 % buffer A, 20 % buffer B, 5 min; 0 % buffer A, 100 % buffer B, 10 min; 100 % buffer A, 0 % buffer B, 15 min (buffer A, water with 0.1 % formic acid; buffer B, acetonitrile with 0.1 % formic acid). The flow rate was 0.7 ml/min.

HPLC purification of reaction products

Reaction mixtures were boiled, cooled on ice and centrifuged. The supernatants were analyzed using SphereClone 5 μm SAX HPLC column (250 mm × 4.6 mm; Phenomenex). The column was pre-equilibrated with 30 mM KH_2PO_4, pH 4.33. For each run, 100 μl of sample was injected and eluted using buffer (30 mM potassium phosphate buffer, pH 4.33) over 30 min at a flow rate of 1 ml/min. NDP-sugars were detected based on their A_{254} values. The retention times for dTDP-Glc, dTDP-rhamnose, UDP-Glc and UDP-rhamnose were 14.8 min, 16.4 min, 12.4 min and 13.9 min, respectively.

NMR spectrometry of reaction products

Overnight reaction mixtures (1 ml) were HPLC-purified to produce dTDP-Glc (~500 μg), UDP-Glc (~500 μg), dTDP-rhamnose (~400 μg) and UDP-rhamnose (~300 μg). Products were lyophilized, dissolved in 99.9 % ^2H_2O (Cambridge Isotopes) and analyzed by water-suppressed ^1H and COSY NMR spectroscopy on a Bruker Advance II 600 MHz NMR spectrometer, equipped with a 5 mm TXI cryoprobe. Chemical shifts of spectra are expressed in p.p.m. referenced to the internal water (4.800 p.p.m.). NMR data were processed using MestReNova software.

Sugar nucleotide analysis

For extraction of sugar nucleotides, we adapted a previously published method [32]. Wild-type worms were cultured in 150 ml of the axenic semi-defined medium CeHR [33] for 7 days. Alternatively, *rrf-3* worms were cultured in S medium (150 ml) with IPTG-induced RNAi strains, including L4440 (control), *rml-2* or *rml-3*, for 9 days. All worms were collected and washed with M9 buffer three times over 3 h to allow the worms to eliminate waste from their digestive track. Worm samples were then frozen using liquid nitrogen, lyophilized, ground with sand and a mortar and pestle and dissolved with 15 ml of 80 % ethanol in M9 buffer. Sugar nucleotides were extracted by vortex-mixing, sonicating for 10 min and shaking for another 3 h. Samples were then centrifuged at 2671 ***g*** for 10 min and then at 38 828 ***g*** for 25 min. The supernatants were filtered through a 0.22 μm filter, dried using a SpeedVac, resuspended in 100 μl of 20 mM triethylammonium acetate (TEAA) buffer, pH 6.0, and centrifuged at 21 130 ***g*** for 10 min. The resulting crude sugar nucleotide samples were stored at −80 °C before analysis by LC–MS, LC–MS/MS and LC–MS/MS/MS. Sugar nucleotide standards UDP-Glc, UDP-galactose (UDP-Gal), UDP-*N*-acetyl-glucosamine (UDP-GlcNAc) and GDP-mannose

(GDP-Man) were purchased from Sigma. UDP-rhamnose, dTDP-Glc and dTDP-rhamnose were enzymatically synthesized and purified as described above. LC–MS analysis was performed as described above, but with a different solvent gradient: 100 % buffer A, 0 % buffer B, 0 min; 100 % buffer A, 0 % buffer B, 15 min; 50 % buffer A, 50 % buffer B, 35 min; 0 % buffer A, 100 % buffer B, 42 min; 100 % buffer A, 0 % buffer B, 44 min; 100 % buffer A, 0 % buffer B, 49 min (buffer A, 20 mM TEAA buffer, pH 6.0; buffer B, 4 % acetonitrile in 20 mM TEAA buffer, pH 6.0) [34]. The flow rate was 1 ml/min. At least three independent experiments were performed for each worm strain to determine the relative amount of each sugar nucleotide. LC–MS/MS and LC–MS/MS/MS were run on a Thermo Scientific LCQ Deca Ion Trap instrument coupled with a Hypersil Gold aQ C_{18} column (150 mm × 2.1 mm; particle size 3 μm; Thermo Scientific) with the same solvent gradient as the LC–MS above, but with a lower flow rate of 0.25 ml/min. Selected ion monitoring (SIM) was performed first on the component of interest, $[M - H]^-$ at *m*/*z* 547 or 533. A selected ion chromatogram of the MS/MS fragment at *m*/*z* 321 or 323 was extracted for MS/MS, and a further fragmentation was performed at *m*/*z* 321 for MS/MS/MS (MS^3).

Ascaroside analysis

Ascaroside production was analyzed using a previously published method [35]. At least three independent experiments were conducted for each assay.

Plasmid construction, transgenesis and microscopy

~2 kb of the *rml-2* or *rml-4* promoter was amplified by PCR from *C. elegans* genomic DNA using the primers listed in Supplementary Table S1. The promoters were inserted into the AscI/NotI (for *rml-2*) or SalI/NotI (for *rml-4*) sites of pPD114.108 (Addgene) to obtain *prml-2::gfp* or *prml-4::gfp*. To generate *prml-2::gfp-pest* for monitoring dynamic expression, the *pest* sequence from pAF207 (gift from Alison Frand, University of California Los Angeles, Los Angeles, CA, U.S.A.) was subcloned into *prml-2::gfp* using the XhoI/EcoRI sites. To generate *prml-4::gfp-pest*, the *pest* sequence was first subcloned into pPD114.108 using the XhoI/EcoRI sites to obtain pPD114.108-GFP-*pest*, and then the *rml-4* promoter was inserted into pPD114.108-GFP-*pest* at the SalI/NotI sites. Microinjections into N2 worms were conducted as described previously [36], using an injection mixture containing 50 ng/μl of either *prml-2::gfp, prml-2::gfp-pest, prml-4::gfp* or *prml-4::gfp-pest* and 50 ng/μl co-injection marker *coel::dsRED* (gift from Piali Sengupta, Brandeis University, Waltham, MA, U.S.A.). At least five independent lines were analyzed. To generate synchronized L1 worms, gravid transgenic *prml-2::gfp, prml-2::gfp-pest, prml-4::gfp* or *prml-4::gfp-pest* worms were treated with alkaline bleach to obtain eggs, which were washed twice with water and once with M9, and then allowed to hatch for 18 h in M9 buffer with shaking at 225 rev./min and 22.5 °C. To monitor GFP expression during the molting cycle, 20 synchronized L1 worms (containing the *prml-2::gfp-pest* or *prml-4::gfp-pest* reporter) were seeded on to an NGM agar plate with OP50 at 22.5 °C. Worms expressing the fluorescent reporters (n = 25) were selected and moved on to a new NGM plate with OP50 at 22.5 °C, and the time course was initiated. GFP expression was recorded every 2 h on a Zeiss Axiovert.A1 microscope equipped with a ZEN lite 2012 camera. For examination of gene expression in pre-dauers and dauers, dauer formation was induced as described in [37]. Dauers were examined 64–72 h after egg laying, and pre-dauers were examined 40–64 h after egg laying.

Table 1 Observed phenotypes for RNAi of genes

Gene	Phenotypes
rml-1 (K08E3.5)	Embryonic lethal [63,64] (the present study); extended lifespan [65]; larval arrest [63] (the present study); slow growth [64]; transgene subcellular localization variant [66]
gmp-1 (C42C1.5)	Adult lethal [64]; embryonic lethal [64] (the present study); larval arrest [67] (the present study); larval lethal [64]; maternal sterile [63]
ugp-1 (D1005.2)	None
rml-2 (F53B1.4)	Sluggish [67]
rml-3 (C14F11.6)	Bordering at edges of RNAi bacterial lawns (the present study)
rml-4 (C01F1.3)	Early larval arrest [68]; egg-laying variant [63]; larval arrest [67] (the present study); larval lethal [67]; lethal [69]; locomotion variant [67]; embryonic lethal (the present study)
rml-5 (Y71G12B.6)	Embryonic lethal [68]

RESULTS

BLAST analysis and observed phenotypes for genes

To investigate whether a rhamnose biosynthetic pathway is present in *C. elegans*, we used BLAST analysis. We first identified three possible NDP-sugar pyrophosphorylases, *rml-1* (K08E3.5), *gmp-1* (C42C1.5) and *ugp-1* (D1005.2), which usually catalyze the conjugation of Glc-1-P or Man-1-P to NTP to give NDP-Glc or NDP-Man, respectively. Of these three genes, *rml-1* and *gmp-1* are essential in embryogenesis and larval development based on observed phenotypes in RNAi experiments or in mutants [38] (Table 1). For the additional steps in NDP-rhamnose biosynthesis, *RmlB*, *RmlC* and *RmlD* from *E. coli* [39] and *RHM2* and *UER1* from *Arabidopsis thaliana* [17] were used to obtain putative 4,6-dehydratase, 3,5-epimerase and 4-keto-reductase homologs in *C. elegans*, *rml-2* (F53B1.4), *rml-3* (C14F11.6) and *rml-4* (C01F1.3), respectively. Whereas RNAi against *rml-2* and *rml-3* does not affect embryonic or larval development, *rml-4* RNAi or gene deletion causes lethality and sterility in worms (Table 1). Homologs of these genes can be found in both free-living and parasitic nematode species (Figures 1A–1E), suggesting that these genes play a conserved role through nematode evolution.

Characterization and enzymatic properties of RML-1, GMP-1 and UGP-1

RML-1, UGP-1 and GMP-1 were expressed in *E. coli* and purified using nickel-affinity resin and then gel filtration (Figure 2A, lanes 1–3). Although RML-1 and UGP-1 are both annotated as UDP-Glc pyrophosphorylases, they showed very different substrate specificities. RML-1 demonstrated a broad substrate range toward five nucleotides (dTTP, UTP, CTP, ATP and GTP) in the presence of Glc-1-P, with higher activity toward dTTP and UTP, and with very low activity toward UTP with Man-1-P (Figure 2B). UGP-1 was specifically active toward UTP with Glc-1-P, but displayed very low or no activity toward other nucleotides, with either Glc-1-P or Man-1-P (Figure 2C). GMP-1 was specifically active toward GTP in the presence of Glc-1-P or Man-1-P, although it preferred Man-1-P. GMP-1 showed almost no activity toward the other nucleotides (Figure 2D). The kinetic parameters of the three enzymes toward different substrates are summarized in Table 2.

RML-2 is a dTDP-Glc 4,6-dehydratase

We identified RML-2, which belongs to the short-chain dehydrogenase/reductase (SDR) family, as a potential second

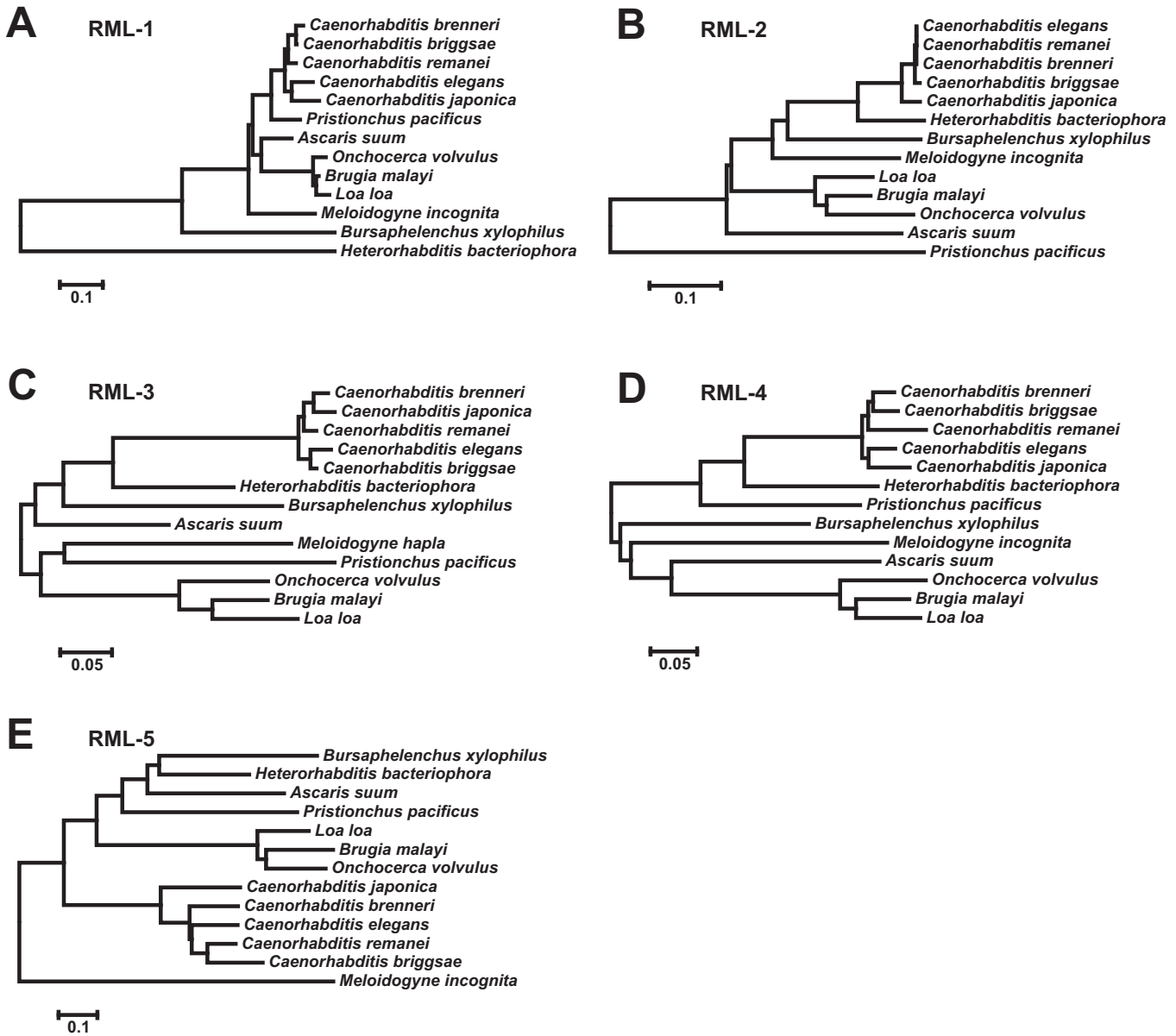

Figure 1 RML-1–5 homologs from different nematode species organized in neighbor-joining phylogenetic trees

The phylogenetic trees were generated by MEGA 6.0 using sequences of RML-1–5 homologs from 13 nematode species. The following sequences were acquired from Wormbase: (**A**) *C. elegans* RML-1 and its homologs, *Caenorhabditis remanei* CRE04853, *Caenorhabditis japonica* CJA03580, *Caenorhabditis brenneri* CBN11066, *Caenorhabditis briggsae* CBG18265, *Pristionchus pacificus* PPA08493, *Brugia malayi* Bm13963, *Onchocerca volvulus* OVOC8721, *Bursaphelenchus xylophilus* BX:BUX.s01142.24, *Heterorhabditis bacteriophora* HB:Hba_01354, *Loa loa* LL:EFO21664.1, *Ascaris suum* AS:GS_14768 and *Meloidogyne incognita* MI:Minc03247. (**B**) *C. elegans* RML-2 and its homologs, *C. remanei* CRE00931, *C. japonica* CJA12429, *C. brenneri* CBN25184, *C. briggsae* CBG14085, *P. pacificus* PPA20960, *B. malayi* Bm9898, *O. volvulus* OVOC2669, *B. xylophilus* BX:BUX.s01144.243, *H. bacteriophora* HB:Hba_07512, *L. loa* LL:EFO24845.2, *A. suum* AS:GS_19609 and *M. incognita* MI:Minc05550. (**C**) *C. elegans* RML-3 and its homologs, *C. remanei* CRE00181, *C. japonica* CJA08012, *C. brenneri* CBN15172, *C. briggsae* CBG05010, *P. pacificus* PPA18087, *B. malayi* Bm2207, *O. volvulus* OVOC3044, *B. xylophilus* BX:BUX.s01355.1, *H. bacteriophora* HB:Hba_14212, *L. loa* LL:EFO28373.1, *A. suum* AS:GS_17184 and *M. hapla* MH:MhA1_Contig1.frz3.fgene1. (**D**) *C. elegans* RML-4 and its homologs, *C. remanei* CRE22549, *C. japonica* CJA06599, *C. brenneri* CBN09988, *C. briggsae* CBG03656, *P. pacificus* PPA20960, *B. malayi* Bm1876, *O. volvulus* OVOC10817, *B. xylophilus* BX:BUX.s00351.21, *H. bacteriophora* HB:Hba_20989, *L. loa* LL:EJD75859.1, *A. suum* AS:GS_21000 and *M. incognita* MI:Minc01529. (**E**) *C. elegans* RML-5 and its homologs, *C. remanei* CRE03894, *C. japonica* CJA06758, *C. brenneri* CBN19366, *C. briggsae* CBG22228, *P. pacificus* PPA01693, *B. malayi* Bm10271, *O. volvulus* OVOC1741, *B. xylophilus* BX:BUX.s00055.268, *H. bacteriophora* HB:Hba_07918, *L. loa* LL:EFO20509.2, *A. suum* AS:ASU_05503 and *M. incognita* MI:Minc14214.

enzyme in the rhamnose biosynthetic pathway. Similar to homologs such as the dTDP-Glc 4,6-dehydratases in *E. coli* (RmlB) and in humans, RML-2 contains a Rossmann domain with the conserved NAD^+-binding motif GXXGXXG ($G^{15}GCGFIG^{21}$), as well as the catalytic site YXXXK ($Y^{164}AASK^{168}$), both of which are essential for the catalytic activity of this type of enzyme. RML-2 was overexpressed in *E. coli* and purified (Figure 2A, lane 4). To test which NDP-glucose was the optimal substrate for RML-2, different kinds of NDP-glucose were prepared from RML-1-, GMP-1- or UGP-1-catalyzed overnight reactions. Aliquots of the reaction mixtures were incubated with RML-2 in the presence of the cofactor

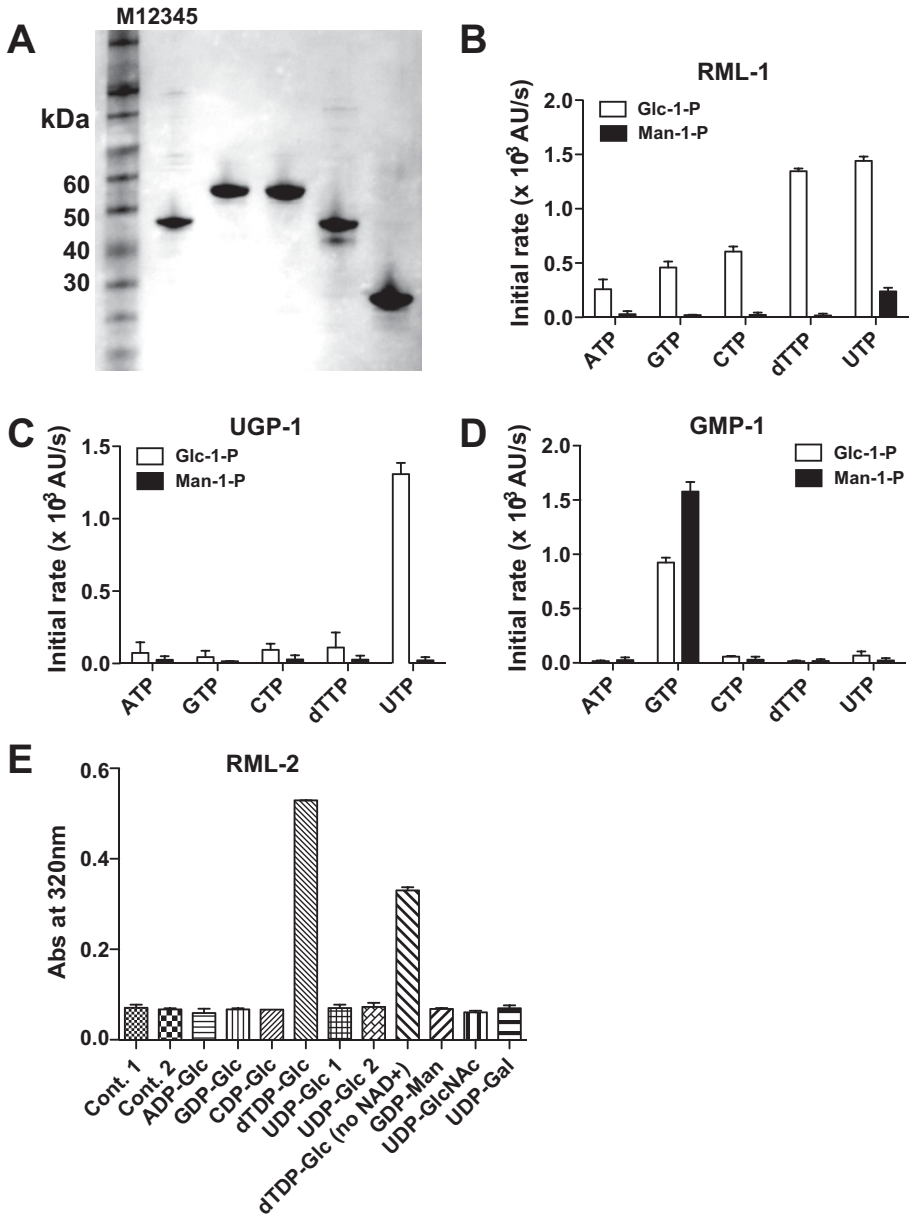

Figure 2 Activity assays with RML-1, GMP-1, UGP-1 and RML-2

(**A**) SDS/PAGE analysis of purified protein, lane M, molecular mass marker; lane 1, GMP-1; lane 2, UGP-1; lane 3, RML-1; lane 4, RML-2; lane 5, RML-3. (**B**–**D**) Substrate specificity of RML-1, UGP-1 and GMP-1. Enzymatic activities were determined for five different NTPs (1 mM ATP, GTP, CTP, dTTP or UTP) in the presence of 1 mM substrates Glc-1-P or Man-1-P. (**E**) Substrate specificity of RML-2. Substrate ADP-Glc, CDP-Glc, dTDP-Glc or UDP-Glc 1 was generated from a RML-1-catalyzed reaction of ATP, CTP, dTTP or UTP and Glc-1-P. GDP-Glc was from a GMP-1-catalyzed reaction of GTP and Glc-1-P. UDP-Glc 2 was from a UGP-1-catalyzed reaction of UTP and Glc-1-P. GDP-Man, UDP-GlcNAc and UDP-Gal are commercially available. Negative controls were reaction mixtures without either RML-2 (Cont. 1) or pyrophosphorylase (Cont. 2). The data in (**B**), (**C**), (**D**) and (**E**) are the averages (±S.D.) for three independent experiments.

NAD^+, and reaction products were monitored by measuring the absorbance at 320 nm under alkaline conditions [28]. RML-2 was specifically active toward dTDP-Glc, showing little, if any, activity toward UDP-Glc and no activity toward other potential NDP-glucose substrates or toward several NDP-sugars that are abundant in *C. elegans* (e.g. GDP-Man, UDP-GlcNAc and UDP-Gal) (Figure 2E). The product of the reaction of RML-2 with dTDP-Glc was analyzed by LC–MS, demonstrating conversion of dTDP-Glc (*m*/*z* 563) into dTDP-4-keto-6-deoxyglucose (*m*/*z* 545) (results not shown). Even when no exogenous NAD^+ was provided, RML-2 still displayed activity toward dTDP-Glc (Figure 2E, dTDP-Glc, no NAD^+). A similar result has also been seen for other NDP-Glc 4,6-dehydratases, which have been shown to bind their NAD^+ cofactors tightly during purification [40,41].

Domain analysis of RML-4

RML-4 was identified as a potential fourth enzyme in the rhamnose biosynthetic pathway using BLAST analysis with the NDP-rhamnose biosynthetic genes RHM2 from *A. thaliana* and RmlB from *S. suis*. After amino acid sequence alignment, we compared the domains of RML-4, *At*RHM2, *Ss*RmlB and RML-2 (Figure 3A). RML-4 has two Rossmann folds with the conserved

Table 2 Kinetic parameters of RML-1, GMP-1 and UGP-1 in the pyrophosphorylase activity assay

Kinetic parameters were determined with different concentrations of sugar 1-phosphate (Glc-1-P or Man-1-P) or NTP (GTP/UTP/dTTP), whereas concentrations of NTP or sugar 1-phosphate were fixed. K_m and k_{cat} are given as mean ± S.D. from three replicates, and the S.D. of k_{cat}/K_m was calculated using the Fenner formula [27].

Enzyme	Substrate	K_m (μM)	k_{cat} (s^{-1})	k_{cat}/K_m ($\mu M^{-1} \cdot s^{-1}$)
RML-1	UTP (Glc-1-P)	9.47 ± 1.70	21.92 ± 0.61	2.31 ± 0.42
	dTTP (Glc-1-P)	24.22 ± 2.86	28.20 ± 0.76	1.16 ± 0.14
	Glc-1-P (UTP)	32.24 ± 3.65	23.24 ± 0.58	0.72 ± 0.084
	Glc-1-P (dTTP)	49.88 ± 4.14	23.58 ± 0.47	0.47 ± 0.040
GMP-1	GTP (Glc-1-P)	88.98 ± 11.95	27.96 ± 1.27	0.31 ± 0.045
	GTP (Man-1-P)	16.04 ± 1.68	29.05 ± 0.58	1.81 ± 0.19
	Glc-1-P (GTP)	508.90 ± 118.40	33.10 ± 2.90	0.065 ± 0.016
	Man-1-P (GTP)	18.49 ± 2.14	30.31 ± 0.69	1.64 ± 0.19
UGP-1	UTP (Glc-1-P)	13.85 ± 2.95	20.02 ± 0.70	1.45 ± 0.31
	Glc-1-P (UTP)	77.65 ± 7.73	22.96 ± 0.65	0.30 ± 0.031

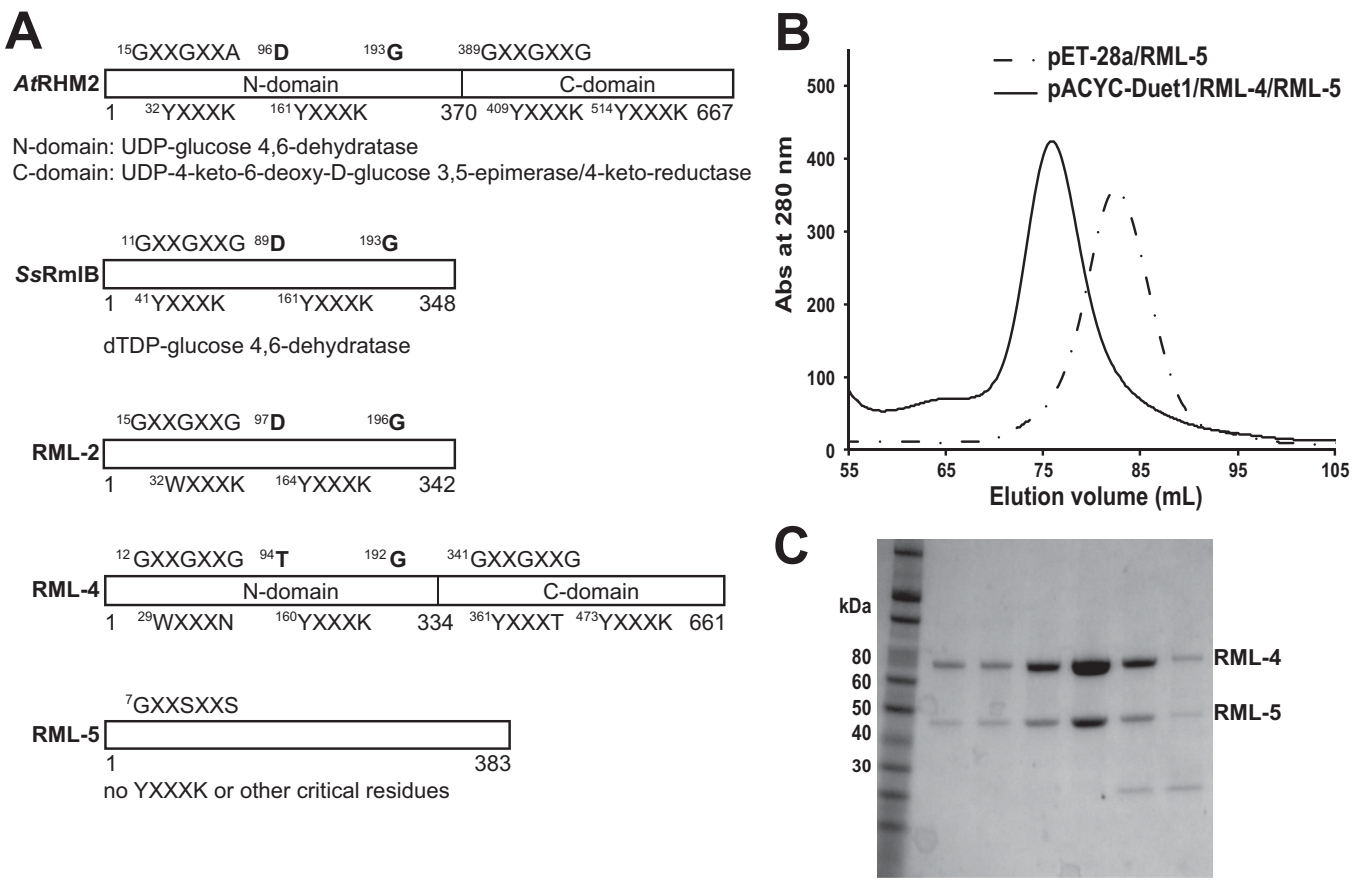

Figure 3 Comparison of the domain structure of RML-4 with known dehydratases and co-expression of RML-4–RML-5

(**A**) Comparison of the domain structures of RML-4 from *C. elegans*, RHM2 from *A. thaliana* (TAIR locus number At1g53500), RmlB in *S. suis* (GenBank accession number BAM95117), RML-2 and RML-5 from *C. elegans*. Amino acids shown are the putative conserved NAD(P)$^+$-binding motif GXXGXXG/A, the catalytic motif YXXXK and other residues that are essential for enzymatic activity (e.g. in *At*RHM2, the D96N and G193A mutations were shown to completely abolish the dehydratase activity). (**B**) Gel-filtration chromatograms of N-terminal His-tagged RML-5 in pET28a (dashed line) and N-terminal His-tagged RML-4 and RML-5 with no tag in pACYC-Duet1 (continuous line). (**C**) SDS/PAGE analysis of gel-filtration fractions containing the RML-4–RML-5 complex. Upper band indicates RML-4 (72 kDa) and lower band indicates RML-5 (41.9 kDa).

motifs GXXGXXG and YXXXK, one in its N-terminal domain and one in its C-terminal domain. RML-4 shares 28.97 % identity with *At*RHM2, in which the N-terminal domain (amino acids 1–370) is an UDP-Glc 4,6-dehydratase and the C-terminal domain (amino acids 371–667) is a bifunctional UDP-4-keto-6-deoxy-glucose 3,5-epimerase/4-keto-reductase [17]. The N-terminal domain of RML-4 (amino acids 1–334) shares approximately 28 % identity with *Ss*RmlB and RML-2, which have both been shown to be dTDP-Glc 4,6-dehydratases. It is important to note that the dehydratase activity of *At*RHM2 has been shown to require, in addition to the essential residues in the Rossmann fold, two other residues, Asp^{96} and G^{193} [17]. The glycine and aspartate residues are conserved in *At*RHM2, *Ss*RmlB and RML-2. Intriguingly, however, although the glycine residue

in RML-4 is conserved, the aspartate residue is replaced by threonine. This substitution potentially indicates that, unlike the *At*RHM2 N-terminal domain, *Ss*RmlB or RML-2, RML-4 may have attenuated or no dehydratase activity. To further investigate the possible role of the aspartate residue in *At*RHM2, *Ss*RmlB and RML-2, and the effect of replacing with threonine on RML-4 activity, we used Robetta to predict the structure of full-length RML-4 (amino acids 1–631). *Ss*RmlB without substrate bound (PDB code 1OC2) was selected as the template for RML-4 N-terminal domain (amino acids 1–344) modeling and *Ec*RmlD (PDB code 1KBZ) was selected as the template for RML-4 C-terminal domain (amino acids 345–631) modeling. Modeling suggested that the N-terminal domain of RML-4 has very similar secondary and tertiary structural folds to those of the well-characterized dehydratases. Structural alignment suggests that the aspartate residue may play a crucial role in stabilizing and/or recognizing the substrate dTDP-Glc or UDP-Glc (Supplementary Figure S1). Thus, replacing the aspartate residue in *At*RHM2, *Ss*RmlB and RML-2 with threonine in RML-4 may disrupt the dehydratase activity of RML-4.

Expression of RML-4

We attempted to express RML-4 with either an N- or C-terminal His, GST or MBP tag, but we were unable to express the enzyme in a stable form. Analysis of *rml-4* with the Spell [42] and String [43] databases indicated that the gene is transcriptionally correlated with *rml-5* (Y71G12B.6). Sequence analysis suggests that RML-5 is a member of the NAD-dependent epimerase/dehydratase family; however, it lacks the conserved motifs GXXGXXG and YXXXK. As with *rml-4*, loss of *rml-5* gene function results in an embryonic lethal phenotype (Table 1). We hypothesized that RML-4 and RML-5 might work together. RML-5 could be overexpressed and purified alone, and, furthermore, co-expression of RML-5 with N-terminal His-tagged RML-4 enabled the purification of stable RML-4 as a RML-4–RML-5 complex (Figures 3B and 3C).

Enzymatic studies of RML-4–RML-5

Given that the N-terminal domains of RML-4 and RML-5 have homology to dehydratases (but lack catalytically important motifs/residues), we first determined whether they had any dehydratase activity. Comparison of dehydratase activities of RML-2 and RML-4–RML-5 on dTDP-Glc and UDP-Glc showed that RML-4–RML-5 had very low, if any, activity on the two substrates (Figure 4A). We did not detect any dehydratase activity of RML-4–RML-5 on other sugar nucleotide (e.g. ADP-Glc, CDP-Glc or GDP-Glc, UDP-Gal, GDP-Man or UDP-GlcNAc). We also did not detect any dehydratase activity for RML-5 alone on various NDP-Glc substrates based on LC–MS analysis (results not shown).

Before testing the potential reductase activity of the RML-4–RML-5 complex, we cloned, expressed and purified a potential third enzyme in the rhamnose biosynthetic pathway, RML-3, a predicted 3,5-epimerase which shares 41.33 % identity with RmlC, a well-characterized dTDP-4-keto-6-deoxyglucose/dTDP-4-dehydrorhamnose 3,5-epimerase (Figure 2A, lane 5, and Supplementary Figure S2). The reductase activity of the RML-4–RML-5 complex toward dTDP-4-keto-6-deoxyglucose (produced by reaction of RML-2 with dTDP-Glc) was monitored by measuring NAD(P)H consumption. Reductase activity toward dTDP-4-keto-6-deoxyglucose was observed, but only when both RML-4–RML-5 and RML-3 were added to the reaction mixture in the presence of NAD(P)H (Figure 4B). Monitoring the reaction by LC–MS indicated conversion of dTDP-Glc (*m*/*z* 563) into dTDP-4-keto-6-deoxyglucose (*m*/*z* 545) by RML-2, and, subsequently, upon addition of RML-3 and RML-4–RML-5, reduction of the dTDP-4-keto-6-deoxyglucose (to give *m*/*z* 547). Similarly, we could also detect consumption of NAD(P)H in the presence of UDP-Glc only when RML-2, RML-3 and RML-4–RML-5 were all present in the reaction mixture (Figure 4C). Formation of the product of this reaction was verified using LC–MS by showing some conversion of UDP-Glc (*m*/*z* 565) into UDP-4-keto-6-deoxyglucose (*m*/*z* 547) by RML-2, and, subsequently, upon addition of RML-3 and RML-4–RML-5, reduction of the UDP-4-keto-6-deoxyglucose (to give *m*/*z* 549). These results show that RML-3 may catalyze the 3,5-epimerization reaction and that the RML-4–RML-5 complex functions only on the epimerized product as a 4-keto-reductase. Although UDP-Glc is not a good substrate for RML-2, inclusion of subsequent enzymes in the sequence, RML-3 and RML-4–RML-5, probably pulls the reaction forward, allowing production of the final product (*m*/*z* 549).

Characterization of the RML-4–RML-5 reaction products by NMR spectroscopy

The product of the reaction of RML-3 and RML-4–RML-5 with dTDP-4-keto-6-deoxyglucose (generated from the reaction of RML-2 with dTDP-Glc) was purified by HPLC (based on detection of *m*/*z* 547 by LC–MS) for analysis using NMR spectroscopy (Supplementary Figure S3A). Based on ^{1}H NMR (Supplementary Figure S3B) and COSY (Supplementary Figure S3C) spectra, the chemical shifts and coupling constants of the product dTDP-sugar corresponded to those reported for dTDP-rhamnose [39]. Comparison with the ^{1}H NMR spectrum of dTDP-Glc (Supplementary Figure S3D) showed the appearance of a doublet at 1.21 p.p.m., indicating the presence of the 6″ methyl protons. Coupling constants associated with the H1″ proton were $J_{1'',P}$ 8.70 Hz, indicating that the sugar moiety was the β-anomer. Moreover, the coupling constants $J_{3'',4''}$ 9.66 Hz and $J_{4'',5''}$ 9.60 Hz demonstrated the *trans* configurations of these protons in rhamnose (Supplementary Table S2). Thus, the NMR spectra demonstrate that the final product is dTDP-rhamnose when dTDP-4-keto-6-deoxyglucose is incubated with RML-3 and RML-4–RML-5 in the presence of NAD(P)H. Although the reaction was not as efficient, incubation of UDP-Glc with RML-2, RML-3 and RML-4–RML-5 produced UDP-β-L-rhamnose, as determined by the mass, ^{1}H NMR and COSY spectra (Supplementary Figures S4A–S4D and Supplementary Table S2) [39,44].

dTDP-rhamnose biosynthetic pathway functions *in vivo*

To investigate whether dTDP/UDP-rhamnose is produced *in vivo*, we examined the sugar nucleotide pools in bacteria-fed worms and in worms grown in axenic (no bacteria) CeHR medium by LC–MS. Several common sugar nucleotides in worms were detected, including UDP-GlcNAc, which is the most abundant sugar nucleotide in worms [32], UDP-Glc, UDP-Gal and GDP-Man. dTDP-rhamnose (*m*/*z* 547) was detected both in bacteria-fed worms and in worms grown in CeHR medium, indicating that the bacteria are not the source of dTDP-rhamnose (Supplementary Figures S5–S7). UDP-rhamnose was not detected, and thus, it is likely that the biologically relevant biosynthetic pathway produces dTDP-rhamnose, not UDP-rhamnose. LC–MS/MS and LC–MS/MS/MS of the *m*/*z* 547 parent ion demonstrated that

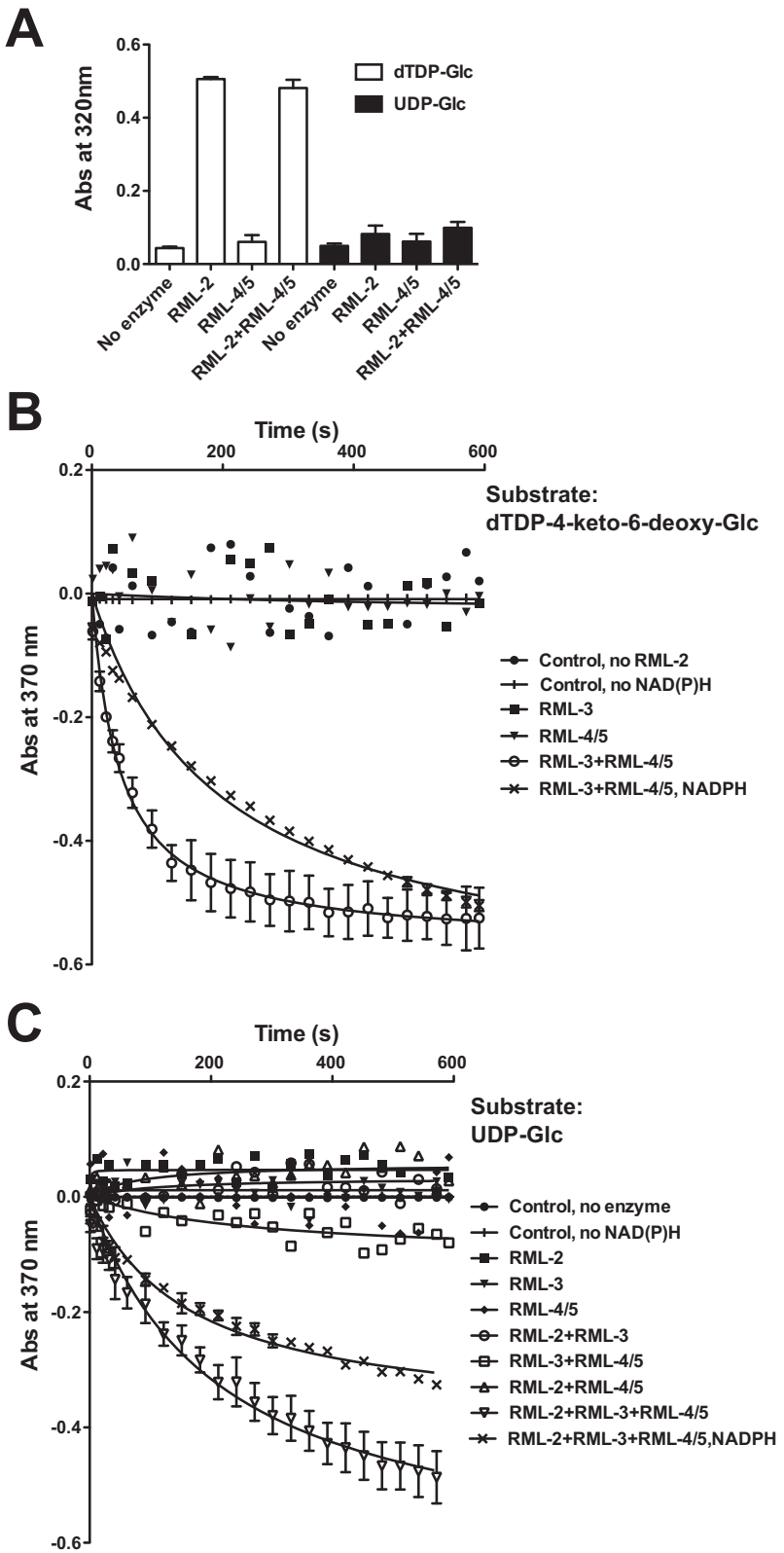

Figure 4 Dehydratase and reductase activities of different enzyme combinations

(**A**) 4,6-Dehydratase activity of RML-2, RML-4–RML-5 or their combinations with either dTDP-Glc (white) or UDP-Glc (black). dTDP-Glc or UDP-Glc was produced by reaction of RML-1 with Glc-1-P and dTTP or UTP. (**B**) RML-4–RML-5 displayed reductase activity (as indicated by a decrease in absorbance at 370 nm) on dTDP-4-keto-6-deoxyglucose (dTDP-4-keto-6-deoxy-Glc) only when RML-3 and NADH (unless noted as NADPH) were present in the mixture. The substrate for the reactions (dTDP-4-keto-6-deoxyglucose) was prepared by overnight pre-incubation of dTDP-Glc (generated using RML-1) with RML-2 and NAD^+ (except in the negative control without RML-2). (**C**) Only when RML-2, RML-3 and RML-4–RML-5 were co-incubated with UDP-Glc, NAD^+ and NADH (unless noted as NADPH) was reductase activity detected (as indicated by a decrease in absorbance at 370 nm).

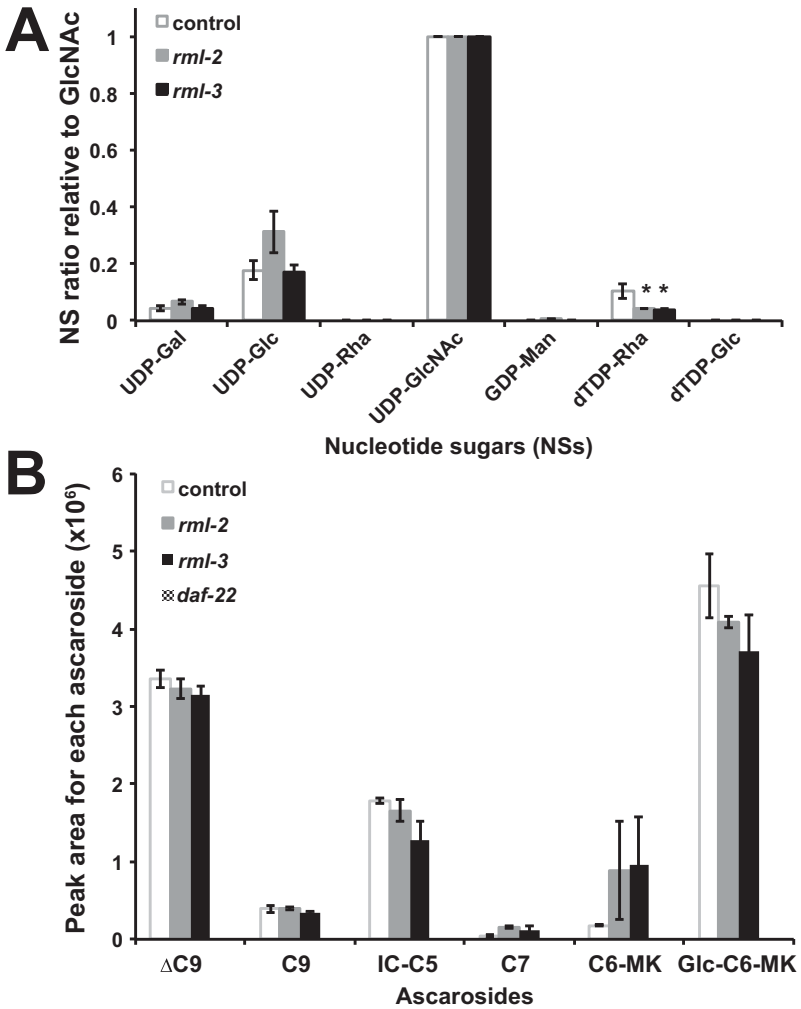

Figure 5 Sugar nucleotide and ascaroside analysis in *C. elegans*

(**A**) Sugar nucleotide analysis in *rrf-3* worms fed with RNAi strains L4440 (control), *rml-2* and *rml-3*. Ion extractions were conducted for each sugar nucleotide, and peak areas were integrated. Each sugar nucleotide was normalized to the NDP-sugar with the highest peak area, UDP-GlcNAc. Two-tailed unpaired Student's *t* tests were conducted to determine the statistical significance for differences in the amount of dTDP-rhamnose (dTDP-Rha) (* indicates $P \leqslant 0.05$). At least three independent experiments were performed. (**B**) LC–MS analysis of ascarosides in the culture medium of *rrf-3* worms fed with RNAi strains L4440 (negative control), *rml-2*, *rml-3* and *daf-22* (positive control). Ascarosides analyzed include asc-ΔC9 (alternative names: C9; ascr#3), asc-C9 (ascr#10), IC-asc-C5 (C5; icas#9), asc-C7 (C7; ascr#1), asc-C6-MK (C6; ascr#2) and Glc-asc-C6-MK (ascr#4).

its fragmentation pattern was consistent with that of dTDP-rhamnose (547→321→195) (Supplementary Figures S8 and S9) [45].

To determine whether the dTDP-rhamnose biosynthetic pathway functions *in vivo*, we knocked down the expression of *rml-2* and *rml-3* by RNAi. Analysis of sugar nucleotides showed that RNAi against either gene significantly reduced production of dTDP-rhamnose, but not other NDP-sugars (Figure 5A). Thus, *rml-2* and *rml-3* contribute *in vivo* to the biosynthesis of dTDP-rhamnose. RNAi against *rml-2* or *rml-3* did not affect the production of the ascarosides, a group of pheromones produced by *C. elegans* to co-ordinate its development and behavior (Figure 5B) [46]. The ascarosides are derivatives of the 3,6-dideoxy-L-sugar ascarylose, which is structurally similar to L-rhamnose but lacks a hydroxy group at the 3-position. Although little is known about the biosynthesis of ascarylose in *C. elegans*, its biosynthesis in bacteria has been extensively studied and includes enzymes that are weakly homologous with the enzymes in the rhamnose biosynthetic pathway, as well as additional enzymes [47,48]. Our data show that ascarylose biosynthesis does not require the rhamnose biosynthetic genes *rml-2* and *rml-3*.

Expression patterns of rml-2 and rml-4 in *C. elegans*

To further investigate the role of rhamnose biosynthesis in *C. elegans*, we generated the transcriptional reporter strains, *prml-2::gfp* and *prml-4::gfp*. The two reporter strains showed very similar GFP expression patterns in embryos (Supplementary Figures S10A and S10B, embryo). In larval stages and the adult, both reporters showed GFP expression in the hypodermal syncytium, but not in the seam cells of the hypodermis (Supplementary Figures S10A and S10B, L1, L2, L3, L4 and adult).

Previous global expression profiling experiments have shown that the expression of *rml-2*, *rml-3*, *rml-4* or *rml-5* changes during molting and a sleep-like lethargus [49]. In addition, these genes

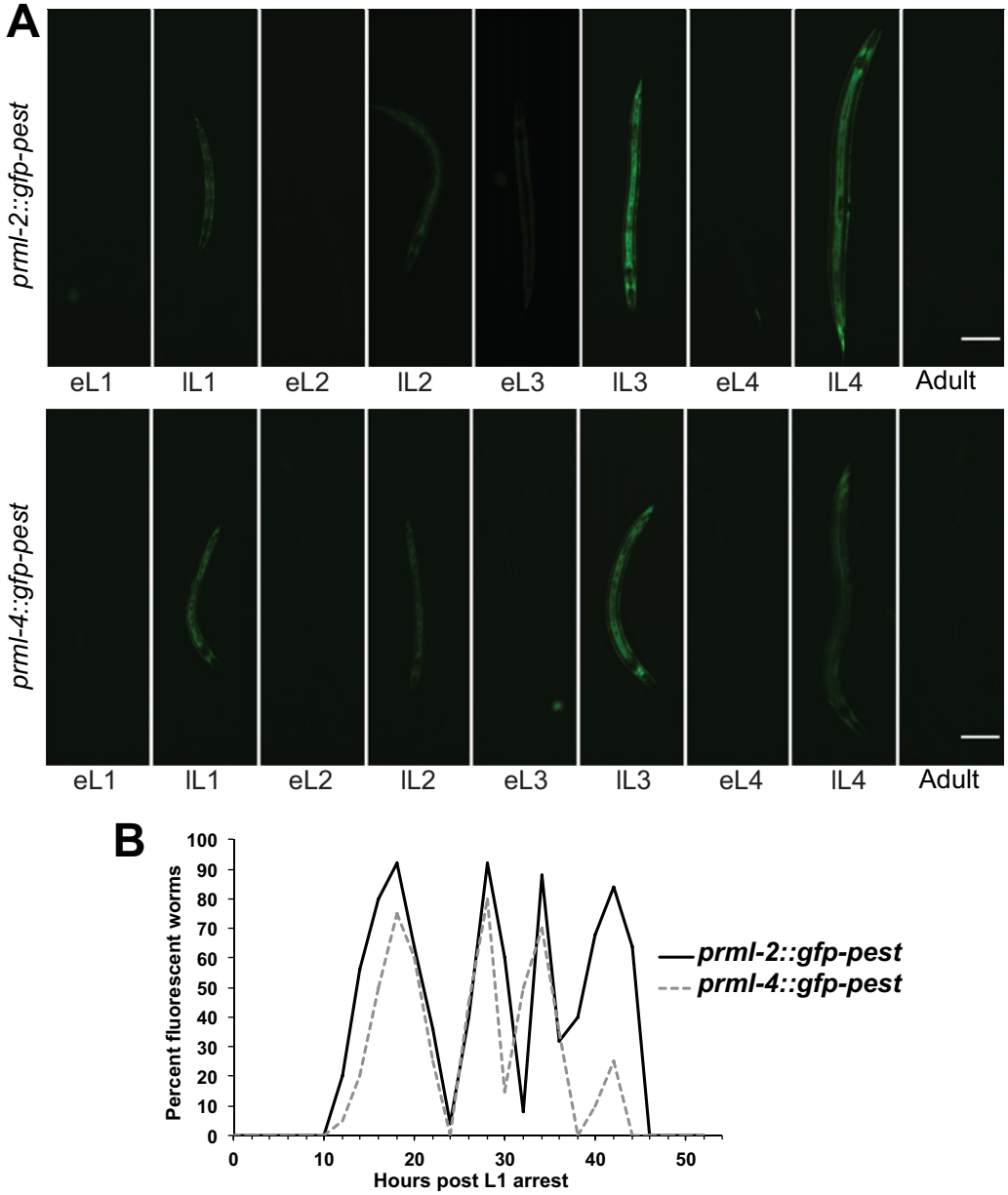

Figure 6 Monitoring the expression of *rml-2* and *rml-4* transcriptional reporters expressing GFP–PEST during the molting cycle

(**A**) The *prml-2::gfp-pest* and *prml-4::gfp-pest* reporter strains expressed GFP as pulses that oscillated with post-embryonic molting. eL1, eL2, eL3 and eL4 represent early L1, L2, L3 and L4 stages, respectively. lL1, lL2, lL3 and lL4 represent late L1, L2, L3 and L4 stages, respectively. Scale bars are 100 μm. (**B**) Percentage of *prml-2::gfp-pest* (continuous line) or *prml-4::gfp-pest* (dashed line) worms that displayed fluorescence. Worms were scored every 2 h post-L1 recovery for fluorescence.

also oscillate during *C. elegans* larval development [50], although *rml-1* expression only showed moderate changes. To verify that the expression of these rhamnose biosynthetic genes is coupled to the worm molting cycle, we employed a destabilized GFP fused to the PEST sequence that results in rapid protein turnover [51–53]. In order to monitor changes in *rml-2* and *rml-4* expression during larval growth, we generated the transcriptional reporters *prml-2::gfp-pest* and *prml-4::gfp-pest*. A pulse of GFP–PEST expression was observed in the hypodermal cells during the later part of each larval stage (lL1, lL2, lL3 and lL4), but not in the early part (eL1, eL2, eL3 and eL4) (Figure 6A). Quantification of GFP–PEST expression during the post-embryonic molting cycles also revealed an oscillating pattern (Figure 6B). All of these results indicate that the rhamnose biosynthetic genes play a role in the molting cycle of *C. elegans*.

The *prml-2::gfp-pest* and *prml-4::gfp-pest* reporters were also highly expressed in the embryo (Figure 7A) and in the seam cells of L1 larvae immediately after recovery from starvation-induced L1 arrest (Figure 7B). To investigate whether the *gfp-pest* reporters were expressed in the dauer stage, the strains were induced to form dauers. In the *prml-4::gfp-pest* strain, GFP–PEST was expressed dominantly in the seam cells of pre-dauers (Figure 7C), but was not expressed at all in dauers (Figure 7D). In the *prml-2::gfp-pest* strain, GFP–PEST was also expressed in the seam cells of pre-dauers, although the expression level in the seam cells was variable from worm to worm (Figure 7E, 1–3),

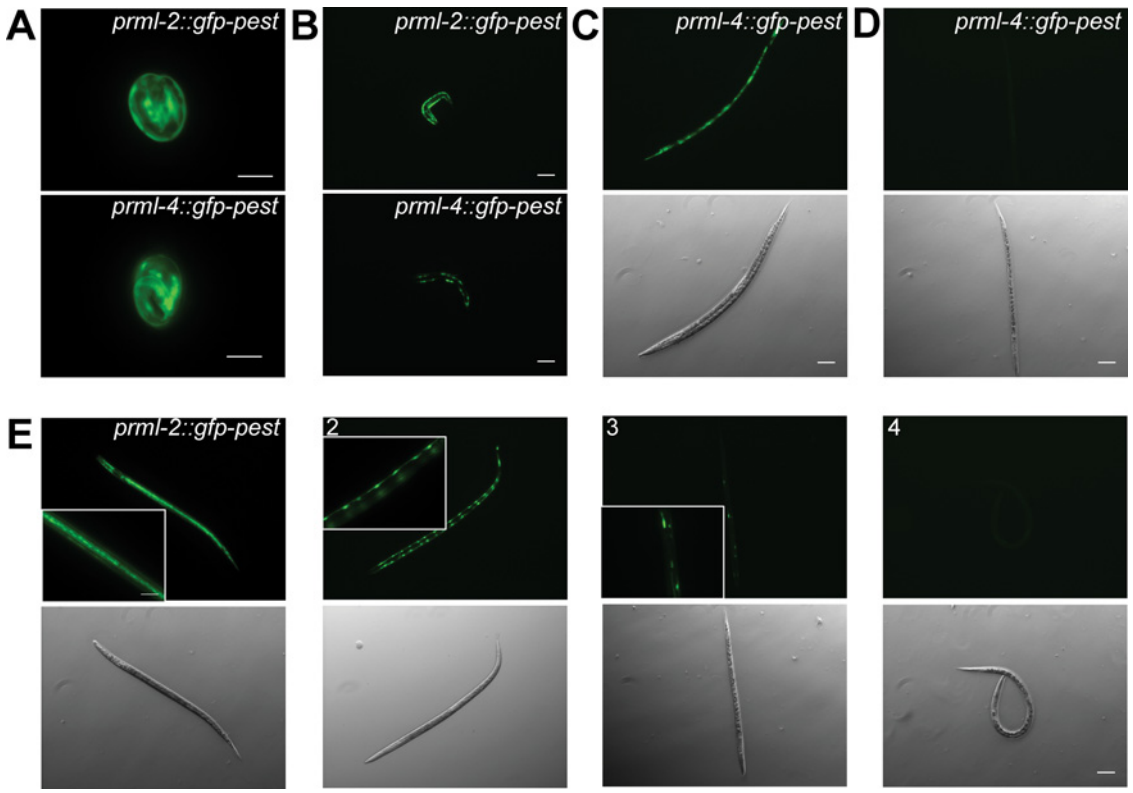

Figure 7 Expression patterns of *prml-2::gfp-pest* and *prml-4::gfp-pest* at specific developmental stages

(**A**) Embryonic stage. Scale bar, 20 μm. (**B**) Very early L1 larvae. Scale bar, 50 μm. (**C**) *prml-4::gfp-pest* in the pre-dauer stage shows GFP expression in seam cells. (**D**) *prml-4::gfp-pest* in the dauer stage shows no GFP expression. Scale bars for (**C**) and (**D**) are 50 μm. (**E**) (1–3) *prml-2::gfp-pest* in the pre-dauer stage shows GFP expression predominantly in the seam cells and (4) *prml-2::gfp-pest* strain in the dauer stage shows no GFP expression. Scale bars are 50 μm and (inset) 20 μm.

and no GFP–PEST was expressed at all in dauers (Figure 7E, 4). As the seam cells are specialized epidermal cells that are critical for cuticle synthesis and molting [21,54], expression of transcriptional reporters for the rhamnose biosynthetic genes in the pre-dauer seam cells may suggest that this biosynthetic pathway is involved in the production of the cuticle and/or surface coat of the dauer stage specifically.

DISCUSSION

In the present study, we uncover a pathway for the biosynthesis of dTDP-rhamnose from dTDP-Glc in *C. elegans* (Figure 8). Our analysis of sugar nucleotide pools in *C. elegans* demonstrated that worms do biosynthesize dTDP-rhamnose *in vivo* and that this biosynthesis requires the rhamnose biosynthetic pathway that we have characterized. Our work is the first to characterize a rhamnose biosynthetic pathway in nematodes or other metazoans. Furthermore, we show that the pathway is specific to the biosynthesis of rhamnose and is not relevant to the biosynthesis of the related 3,6-dideoxy-L-sugar, ascarylose, which is a core component of the ascaroside pheromones in nematodes. As humans cannot biosynthesize rhamnose, but bacteria can, the rhamnose biosynthetic pathway has been proposed as a potential target for the development of new antibiotics. Similarly, the rhamnose biosynthetic pathway in nematodes could be a potential target for new anthelmintics. The identified enzymes in the *C. elegans* pathway, RML-1–5, show very high similarities to their homologs in other nematode species. This conservation suggests an important role for rhamnose in nematodes.

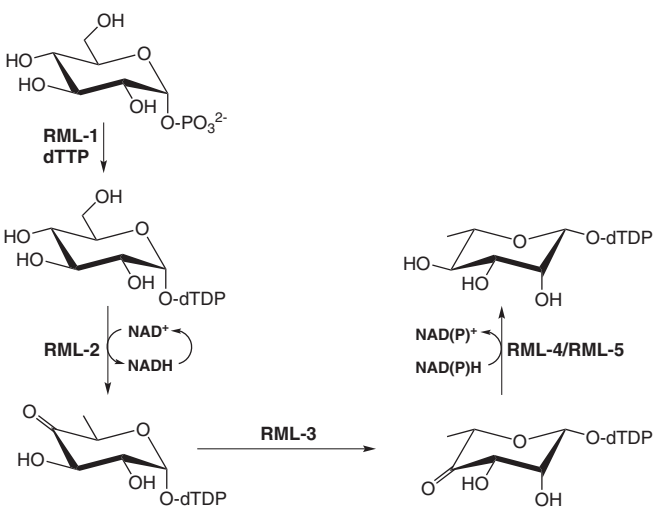

Figure 8 Proposed biosynthetic pathway for dTDP-L-rhamnose in *C. elegans*

Our results show that RML-1 converts Glc-1-P in the presence of dTTP or UTP into dTDP-Glc or UDP-Glc, respectively. The dTDP-Glc is used for the biosynthesis of rhamnose in *C. elegans*, whereas the UDP-Glc may be used in the biosynthesis of glycogen, glycolipids and/or N-glycans [55–57]. A translational reporter for RML-1 has been used to show that this protein is expressed in the intestine, body wall muscle and hypodermis

during larval development, and in the intestine and body wall muscle in the adult worm [58]. Expression of RML-1 in the hypodermis is consistent with our reporter gene data for RML-2 and RML-4, suggesting that rhamnose biosynthesis occurs in the hypodermis. Expression in the muscles is consistent with a role for RML-1 in glycogen biosynthesis. In addition to RML-1, we characterized two other pyrophosphorylases, GMP-1 and UGP-1, and showed that they act as a GDP-Man pyrophosphorylase and an UDP-Glc pyrophosphorylase, respectively. GDP-Man pyrophosphorylase is thought to be involved in the first step of the GDP-fucose (GDP-Fuc) biosynthetic pathway in *C. elegans*, which catalyzes the conjugation of Man-1-P to GMP from GTP. GDP-Man is further transformed by GMD-1 or GMD-2 and GER-1 to form GDP-Fuc, which is used in the biosynthesis of a fucosylated glycolipid that acts as a toxin receptor [59]. Unlike RML-1, the UDP-Glc pyrophosphorylase UGP-1 was previously reported to be strongly up-regulated when worms are exposed to desiccation conditions [60]. UGP-1 was proposed to function in the biosynthesis of trehalose, one component of the maradolipids in the cuticle, which protect worms from harsh environments [61].

The second step in the rhamnose biosynthetic pathway is catalyzed by RML-2, a dTDP-Glc 4,6-dehydratase that converts dTDP-Glc into dTDP-4-keto-6-deoxyglucose. As with other enzymes of the SDR family, such as the dTDP-Glc 4,6-dehydratase RmlB from *E. coli*, RML-2 has the conserved motifs GXXGXXG for NAD^+ cofactor binding and YXXXK for catalysis. Our results show that even if no exogenous NAD^+ is provided, RML-2 still has considerable activity, probably due to the NAD^+ cofactor remaining tightly bound during the purification process. The mechanism of C-6 deoxygenation seen in other NDP-Glc 4,6-dehydratases suggests regeneration of NAD^+ during the reaction cycle of RML-2 [40,62].

The third step in the *C. elegans* rhamnose biosynthetic pathway is catalyzed by RML-3, which we show catalyzes the 3,5-epimerization of dTDP-4-keto-6-deoxyglucose. The last step in the pathway, reduction of the 4-keto group, is catalyzed by RML-4, which could only be co-expressed and purified with RML-5. Although RML-4 has a very similar domain structure to the bifunctional plant enzyme RHM2 (Figure 3A), comparison of the modeled structure of RML-4 with the structure of RmlB suggests that the N-terminal domain of RML-4 is unlikely to have dehydratase activity. In comparison with RmlB, an essential residue in RML-4 has been substituted (aspartate to threonine) that is possibly important for NDP-Glc binding. Indeed, we were not able to detect any significant dehydratase activity for RML-4.

Our data suggest that rhamnose biosynthesis is involved in embryogenesis and in hypodermal development during the post-embryonic molting cycles of *C. elegans*. *C. elegans* molts at the end of each larval stage (L1–L4) and must generate a new cuticle with each molt. Expression of *rml-2* and *rml-4* transcriptional reporters in the hypodermis oscillates with the molting cycle, peaking before each larval molt. It is possible that dTDP-rhamnose in worms is incorporated into glycoproteins or glycolipids during cuticle and/or surface coat synthesis. A previous study claimed that a glycoprotein extracted from the surface of the parasitic nematode *A. galli* contains a rhamnose moiety [23]. Expression of *rml-2* and *rml-4* transcriptional reporters in pre-dauers occurred specifically in the hypodermal seam cells, which are crucial for cuticle production and molting. Thus, rhamnose biosynthesis may be particularly important for the formation of the dauer cuticle and/or surface coat. Phenotypic analysis of genes involved in rhamnose biosynthesis indicates that knockdown of *rml-1*, *rml-4* and *rml-5* (but not *rml-2* and *rml-3*) causes lethality of the embryo. This result may indicate that *rml-2* and *rml-3* work redundantly with other genes in rhamnose biosynthesis, or that *rml-1*, *rml-4* and *rml-5* play an essential role unrelated to rhamnose biosynthesis. The discovery of a rhamnose biosynthetic pathway should enable further discoveries in the role of rhamnose in nematode embryonic/larval development and could possibly facilitate the development of new types of anthelmintics by targeting RML-1, RML-4 or RML-5.

Note added in proof:

F53B1.4/*rml-2* is the same as the uncloned gene *bus-5* (Jonathan Hodgkin, personal communication). *bus-5* is required for colonization by *Microbacterium nematophilum*, fully normal cuticle antigens, cuticle integrity, and long-term survival during starvation [70].

AUTHOR CONTRIBUTION

Likui Feng and Rebecca Butcher conceived the project. Likui Feng performed all experiments. Qingyao Shou obtained and interpreted NMR spectra. Likui Feng and Rebecca Butcher wrote the paper, which was approved by all authors.

ACKNOWLEDGEMENTS

We thank Steven Bruner for providing access to an FPLC and to HPLC columns, Alison Frand and Piali Sengupta for providing plasmids, and Keith Choe and Scott Neal for providing advice on making transgenic strains. We also thank Kari Basso and Jon Allison for tandem mass spectrometry analysis. Some strains were provided by the CGC, which is funded by the National Institutes of Health (NIH) Office of Research Infrastructure Programs (P40 OD010440).

FUNDING

This work was supported by the National Institutes of Health [grant number GM87533 (to R.A.B.)]; the Alfred P. Sloan Foundation [grant number BR2014-071 (to R.A.B.)]; and the University of Florida.

REFERENCES

1 Giraud, M.F. and Naismith, J.H. (2000) The rhamnose pathway. Curr. Opin. Struct. Biol. **10**, 687–696 CrossRef PubMed
2 Kocíncová, D. and Lam, J.S. (2011) Structural diversity of the core oligosaccharide domain of *Pseudomonas aeruginosa* lipopolysaccharide. Biochemistry (Mosc.) **76**, 755–760 CrossRef PubMed
3 Caffall, K.H. and Mohnen, D. (2009) The structure, function, and biosynthesis of plant cell wall pectic polysaccharides. Carbohydr. Res. **344**, 1879–1900 CrossRef PubMed
4 Mohnen, D. (2008) Pectin structure and biosynthesis. Curr. Opin. Plant. Biol. **11**, 266–277 CrossRef PubMed
5 Nguema-Ona, E., Vicré-Gibouin, M., Gotté, M., Plancot, B., Lerouge, P., Bardor, M. and Driouich, A. (2014) Cell wall O-glycoproteins and N-glycoproteins: aspects of biosynthesis and function. Front. Plant Sci. **5**, 499 CrossRef PubMed
6 Allen, S., Richardson, J.M., Mehlert, A. and Ferguson, M.A. (2013) Structure of a complex phosphoglycan epitope from gp72 of *Trypanosoma cruzi*. J. Biol. Chem. **288**, 11093–11105 CrossRef PubMed
7 Allard, S.T., Beis, K., Giraud, M.F., Hegeman, A.D., Gross, J.W., Wilmouth, R.C., Whitfield, C., Graninger, M., Messner, P., Allen, A.G. et al. (2002) Toward a structural understanding of the dehydratase mechanism. Structure **10**, 81–92 CrossRef PubMed
8 He, X. and Liu, H.W. (2002) Mechanisms of enzymatic CbondO bond cleavages in deoxyhexose biosynthesis. Curr. Opin. Chem. Biol. **6**, 590–597 CrossRef PubMed
9 Thibodeaux, C.J., Melançon, C.E. and Liu, H.W. (2007) Unusual sugar biosynthesis and natural product glycodiversification. Nature **446**, 1008–1016 CrossRef PubMed
10 Blankenfeldt, W., Giraud, M.F., Leonard, G., Rahim, R., Creuzenet, C., Lam, J.S. and Naismith, J.H. (2000) The purification, crystallization and preliminary structural characterization of glucose-1-phosphate thymidylyltransferase (RmlA), the first enzyme of the dTDP-L-rhamnose synthesis pathway from *Pseudomonas aeruginosa*. Acta Crystallogr. D Biol. Crystallogr. **56**, 1501–1504 CrossRef PubMed
11 Allard, S.T., Giraud, M.F., Whitfield, C., Messner, P. and Naismith, J.H. (2000) The purification, crystallization and structural elucidation of dTDP-D-glucose 4,6-dehydratase (RmlB), the second enzyme of the dTDP-L-rhamnose synthesis pathway from *Salmonella enterica* serovar typhimurium. Acta Crystallogr. D Biol. Crystallogr. **56**, 222–225 CrossRef PubMed

12 Giraud, M.F., Leonard, G.A., Field, R.A., Berlind, C. and Naismith, J.H. (2000) RmlC, the third enzyme of dTDP-L-rhamnose pathway, is a new class of epimerase. Nat. Struct. Biol. **7**, 398–402 CrossRef PubMed

13 Stern, R.J., Lee, T.Y., Lee, T.J., Yan, W., Scherman, M.S., Vissa, V.D., Kim, S.K., Wanner, B.L. and McNeil, M.R. (1999) Conversion of dTDP-4-keto-6-deoxyglucose to free dTDP-4-keto-rhamnose by the rmlC gene products of *Escherichia coli* and *Mycobacterium tuberculosis*. Microbiology **145**, 663–671 CrossRef PubMed

14 Graninger, M., Nidetzky, B., Heinrichs, D.E., Whitfield, C. and Messner, P. (1999) Characterization of dTDP-4-dehydrorhamnose 3,5-epimerase and dTDP-4-dehydrorhamnose reductase, required for dTDP-L-rhamnose biosynthesis in *Salmonella enterica* serovar Typhimurium LT2. J. Biol. Chem. **274**, 25069–25077 CrossRef PubMed

15 Glaser, L. and Kornfeld, S. (1961) The enzymatic synthesis of thymidine-linked sugars. II. Thymidine diphosphate L-rhamnose. J. Biol. Chem. **236**, 1795–1799 PubMed

16 Giraud, M.F., McMiken, H.J., Leonard, G.A., Messner, P., Whitfield, C. and Naismith, J.H. (1999) Overexpression, purification, crystallization and preliminary structural study of dTDP-6-deoxy-L-lyxo-4-hexulose reductase (RmlD), the fourth enzyme of the dTDP-L-rhamnose synthesis pathway, from *Salmonella enterica* serovar Typhimurium. Acta Crystallogr. D Biol. Crystallogr. **55**, 2043–2046 CrossRef PubMed

17 Oka, T., Nemoto, T. and Jigami, Y. (2007) Functional analysis of *Arabidopsis thaliana* RHM2/MUM4, a multidomain protein involved in UDP-D-glucose to UDP-L-rhamnose conversion. J. Biol. Chem. **282**, 5389–5403 CrossRef PubMed

18 Schachter, H. (2004) Protein glycosylation lessons from *Caenorhabditis elegans*. Curr. Opin. Struct. Biol. **14**, 607–616 CrossRef PubMed

19 Page, A.P. and Johnstone, I.L. (2007) The cuticle. WormBook, ed. The *C. elegans* Research Community, WormBook, http://www.wormbook.org

20 Golden, J.W. and Riddle, D.L. (1982) A pheromone influences larval development in the nematode *Caenorhabditis elegans*. Science **218**, 578–580 CrossRef PubMed

21 Gravato-Nobre, M.J., Stroud, D., O'Rourke, D., Darby, C. and Hodgkin, J. (2011) Glycosylation genes expressed in seam cells determine complex surface properties and bacterial adhesion to the cuticle of *Caenorhabditis elegans*. Genetics **187**, 141–155 CrossRef PubMed

22 Politz, S.M., Philipp, M., Estevez, M., O'Brien, P.J. and Chin, K.J. (1990) Genes that can be mutated to unmask hidden antigenic determinants in the cuticle of the nematode *Caenorhabditis elegans*. Proc. Natl. Acad. Sci. U.S.A. **87**, 2901–2905 CrossRef PubMed

23 Masood, K., Sircar, K.P. and Srivastava, V.M. (1987) Purification and characterization of a glycoprotein from the surface of *Ascaridia galli*. J. Helminthol. **61**, 219–224 CrossRef PubMed

24 Langenhan, T., Prömel, S., Mestek, L., Esmaeili, B., Waller-Evans, H., Hennig, C., Kohara, Y., Avery, L., Vakonakis, I., Schnabel, R. and Russ, A.P. (2009) Latrophilin signaling links anterior-posterior tissue polarity and oriented cell divisions in the *C. elegans* embryo. Dev. Cell **17**, 494–504 CrossRef PubMed

25 Tamura, K., Stecher, G., Peterson, D., Filipski, A. and Kumar, S. (2013) MEGA6: molecular evolutionary genetics analysis version 6.0. Mol. Biol. Evol. **30**, 2725–2729 CrossRef PubMed

26 Timmons, L., Court, D.L. and Fire, A. (2001) Ingestion of bacterially expressed dsRNAs can produce specific and potent genetic interference in *Caenorhabditis elegans*. Gene **263**, 103–112 CrossRef PubMed

27 Fenner, G. (1931) Das Genauigkeitsmaβ von Summen, Differenzen, Produktenund Quotienten der Beobachtungsreichen. Naturwissenschaften **19**, 310 CrossRef

28 Okazaki, R., Okazakit, Strominger, J.L. and Michelson, A.M. (1962) Thymidine diphosphate 4-keto-6-deoxy-D-glucose, an intermediate in thymidine diphosphate L-rhamnose synthesis in *Escherichia coli* strains. J. Biol. Chem. **237**, 3014–3026 PubMed

29 Marquez, L.A. and Dunford, H.B. (1995) Transient and steady-state kinetics of the oxidation of scopoletin by horseradish peroxidase compounds I, II and III in the presence of NADH. Eur. J. Biochem. **233**, 364–371 CrossRef PubMed

30 Read, J.A., Wilkinson, K.W., Tranter, R., Sessions, R.B. and Brady, R.L. (1999) Chloroquine binds in the cofactor binding site of *Plasmodium falciparum* lactate dehydrogenase. J. Biol. Chem. **274**, 10213–10218 CrossRef PubMed

31 Kim, D.E., Chivian, D. and Baker, D. (2004) Protein structure prediction and analysis using the Robetta server. Nucleic Acids Res. **32**, W526–W531 CrossRef PubMed

32 Novelli, J.F., Chaudhary, K., Canovas, J., Benner, J.S., Madinger, C.L., Kelly, P., Hodgkin, J. and Carlow, C.K. (2009) Characterization of the *Caenorhabditis elegans* UDP-galactopyranose mutase homolog *glf-1* reveals an essential role for galactofuranose metabolism in nematode surface coat synthesis. Dev. Biol. **335**, 340–355 CrossRef PubMed

33 Nass, R. and Hamza, I. (2007) The nematode *C. elegans* as an animal model to explore toxicology *in vivo*: solid and axenic growth culture conditions and compound exposure parameters. Curr. Protoc. Toxicol. **Chapter 1**, Unit1.9 PubMed

34 Räbinä, J., Mäki, M., Savilahti, E.M., Järvinen, N., Penttilä, L. and Renkonen, R. (2001) Analysis of nucleotide sugars from cell lysates by ion-pair solid-phase extraction and reversed-phase high-performance liquid chromatography. Glycoconj. J. **18**, 799–805 CrossRef PubMed

35 Zhang, X., Noguez, J.H., Zhou, Y. and Butcher, R.A. (2013) Analysis of ascarosides from *Caenorhabditis elegans* using mass spectrometry and NMR spectroscopy. Methods Mol. Biol. **1068**, 71–92 CrossRef PubMed

36 Mello, C.C., Kramer, J.M., Stinchcomb, D. and Ambros, V. (1991) Efficient gene transfer in *C. elegans*: extrachromosomal maintenance and integration of transforming sequences. EMBO J. **10**, 3959–3970 PubMed

37 Butcher, R.A., Ragains, J.R., Kim, E. and Clardy, J. (2008) A potent dauer pheromone component in *Caenorhabditis elegans* that acts synergistically with other components. Proc. Natl. Acad. Sci. U.S.A. **105**, 14288–14292 CrossRef PubMed

38 Harris, T.W., Antoshechkin, I., Bieri, T., Blasiar, D., Chan, J., Chen, W.J., De La Cruz, N., Davis, P., Duesbury, M., Fang, R. et al. (2010) WormBase: a comprehensive resource for nematode research. Nucleic Acids Res. **38**, D463–D467 CrossRef PubMed

39 Watt, G., Leoff, C., Harper, A.D. and Bar-Peled, M. (2004) A bifunctional 3,5-epimerase/4-keto reductase for nucleotide-rhamnose synthesis in *Arabidopsis*. Plant Physiol. **134**, 1337–1346 CrossRef PubMed

40 Creuzenet, C., Schur, M.J., Li, J., Wakarchuk, W.W. and Lam, J.S. (2000) FlaA1, a new bifunctional UDP-GlcNAc C6 dehydratase/C4 reductase from *Helicobacter pylori*. J. Biol. Chem. **275**, 34873–34880 CrossRef PubMed

41 Vogan, E.M., Bellamacina, C., He, X., Liu, H.W., Ringe, D. and Petsko, G.A. (2004) Crystal structure at 1.8 A resolution of CDP-D-glucose 4,6-dehydratase from *Yersinia pseudotuberculosis*. Biochemistry **43**, 3057–3067 CrossRef PubMed

42 Hibbs, M.A., Hess, D.C., Myers, C.L., Huttenhower, C., Li, K. and Troyanskaya, O.G. (2007) Exploring the functional landscape of gene expression: directed search of large microarray compendia. Bioinformatics **23**, 2692–2699 CrossRef PubMed

43 Franceschini, A., Szklarczyk, D., Frankild, S., Kuhn, M., Simonovic, M., Roth, A., Lin, J., Minguez, P., Bork, P., von Mering, C. and Jensen, L.J. (2013) STRING v9.1: protein–protein interaction networks, with increased coverage and integration. Nucleic Acids Res. **41**, D808–D815 CrossRef PubMed

44 Martinez, V., Ingwers, M., Smith, J., Glushka, J., Yang, T. and Bar-Peled, M. (2012) Biosynthesis of UDP-4-keto-6-deoxyglucose and UDP-rhamnose in pathogenic fungi *Magnaporthe grisea* and *Botryotinia fuckeliana*. J. Biol. Chem. **287**, 879–892 CrossRef PubMed

45 Turnock, D.C. and Ferguson, M.A. (2007) Sugar nucleotide pools of *Trypanosoma brucei*, *Trypanosoma cruzi*, and *Leishmania major*. Eukaryot. Cell **6**, 1450–1463 CrossRef PubMed

46 Edison, A.S. (2009) *Caenorhabditis elegans* pheromones regulate multiple complex behaviors. Curr. Opin. Neurobiol. **19**, 378–388 CrossRef PubMed

47 Zhang, X., Feng, L., Chinta, S., Singh, P., Wang, Y., Nunnery, J.K. and Butcher, R.A. (2015) Acyl-CoA oxidase complexes control the chemical message produced by *Caenorhabditis elegans*. Proc. Natl. Acad. Sci. U.S.A. **112**, 3955–3960 CrossRef PubMed

48 Butcher, R.A., Fujita, M., Schroeder, F.C. and Clardy, J. (2007) Small-molecule pheromones that control dauer development in *Caenorhabditis elegans*. Nat. Chem. Biol. **3**, 420–422 CrossRef PubMed

49 Turek, M. and Bringmann, H. (2014) Gene expression changes of *Caenorhabditis elegans* larvae during molting and sleep-like lethargus. PLoS One **9**, e113269 CrossRef PubMed

50 Hendriks, G.J., Gaidatzis, D., Aeschimann, F. and Großhans, H. (2014) Extensive oscillatory gene expression during *C. elegans* larval development. Mol. Cell **53**, 380–392 CrossRef PubMed

51 Frand, A.R., Russel, S. and Ruvkun, G. (2005) Functional genomic analysis of *C. elegans* molting. PLoS Biol. **3**, e312 CrossRef PubMed

52 Meli, V.S., Osuna, B., Ruvkun, G. and Frand, A.R. (2010) MLT-10 defines a family of DUF644 and proline-rich repeat proteins involved in the molting cycle of *Caenorhabditis elegans*. Mol. Biol. Cell **21**, 1648–1661 CrossRef PubMed

53 Perales, R., King, D.M., Aguirre-Chen, C. and Hammell, C.M. (2014) LIN-42, the *Caenorhabditis elegans* PERIOD homolog, negatively regulates microRNA transcription. PLoS Genet. **10**, e1004486 CrossRef PubMed

54 Partridge, F.A., Tearle, A.W., Gravato-Nobre, M.J., Schafer, W.R. and Hodgkin, J. (2008) The *C. elegans* glycosyltransferase BUS-8 has two distinct and essential roles in epidermal morphogenesis. Dev. Biol. **317**, 549–559 CrossRef PubMed

55 Nomura, K.H., Murata, D., Hayashi, Y., Dejima, K., Mizuguchi, S., Kage-Nakadai, E., Gengyo-Ando, K., Mitani, S., Hirabayashi, Y., Ito, M. and Nomura, K. (2011) Ceramide glucosyltransferase of the nematode *Caenorhabditis elegans* is involved in oocyte formation and in early embryonic cell division. Glycobiology **21**, 834–848 CrossRef PubMed

56 Schiller, B., Hykollari, A., Yan, S., Paschinger, K. and Wilson, I.B. (2012) Complicated N-linked glycans in simple organisms. Biol. Chem. **393**, 661–673 CrossRef PubMed

57 Peng, H.L. and Chang, H.Y. (1993) Cloning of a human liver UDP-glucose pyrophosphorylase cDNA by complementation of the bacterial *galU* mutation. FEBS Lett. **329**, 153–158 CrossRef PubMed

58 van Gemert, A.M., van der Laan, A.M., Pilgram, G.S., Fradkin, L.G., Noordermeer, J.N., Tanke, H.J. and Jost, C.R. (2009) *In vivo* monitoring of mRNA movement in *Drosophila* body wall muscle cells reveals the presence of myofiber domains. PLoS One **4**, e6663 CrossRef PubMed

59 Rhomberg, S., Fuchsluger, C., Rendić, D., Paschinger, K., Jantsch, V., Kosma, P. and Wilson, I.B. (2006) Reconstitution *in vitro* of the GDP-fucose biosynthetic pathways of *Caenorhabditis elegans* and *Drosophila melanogaster*. FEBS J. **273**, 2244–2256 CrossRef PubMed

60 Erkut, C., Vasilj, A., Boland, S., Habermann, B., Shevchenko, A. and Kurzchalia, T.V. (2013) Molecular strategies of the *Caenorhabditis elegans* dauer larva to survive extreme desiccation. PLoS One **8**, e82473 CrossRef PubMed

61 Penkov, S., Mende, F., Zagoriy, V., Erkut, C., Martin, R., Pässler, U., Schuhmann, K., Schwudke, D., Gruner, M., Mäntler, J. et al. (2010) Maradolipids: diacyltrehalose glycolipids specific to dauer larva in *Caenorhabditis elegans*. Angew. Chem. Int. Ed. Engl. **49**, 9430–9435 CrossRef PubMed

62 Sturla, L., Bisso, A., Zanardi, D., Benatti, U., De Flora, A. and Tonetti, M. (1997) Expression, purification and characterization of GDP-D-mannose 4,6-dehydratase from *Escherichia coli*. FEBS Lett. **412**, 126–130 CrossRef PubMed

63 Rual, J.F., Ceron, J., Koreth, J., Hao, T., Nicot, A.S., Hirozane-Kishikawa, T., Vandenhaute, J., Orkin, S.H., Hill, D.E., van den Heuvel, S. and Vidal, M. (2004) Toward improving *Caenorhabditis elegans* phenome mapping with an ORFeome-based RNAi library. Genome Res. **14**, 2162–2168 CrossRef PubMed

64 Kamath, R.S., Fraser, A.G., Dong, Y., Poulin, G., Durbin, R., Gotta, M., Kanapin, A., Le Bot, N., Moreno, S., Sohrmann, M. et al. (2003) Systematic functional analysis of the *Caenorhabditis elegans* genome using RNAi. Nature **421**, 231–237 CrossRef PubMed

65 Hamilton, B., Dong, Y., Shindo, M., Liu, W., Odell, I., Ruvkun, G. and Lee, S.S. (2005) A systematic RNAi screen for longevity genes in *C. elegans*. Genes Dev. **19**, 1544–1555 CrossRef PubMed

66 Winter, J.F., Höpfner, S., Korn, K., Farnung, B.O., Bradshaw, C.R., Marsico, G., Volkmer, M., Habermann, B. and Zerial, M. (2012) *Caenorhabditis elegans* screen reveals role of PAR-5 in RAB-11-recycling endosome positioning and apicobasal cell polarity. Nat. Cell Biol. **14**, 666–676 CrossRef PubMed

67 Simmer, F., Moorman, C., van der Linden, A.M., Kuijk, E., van den Berghe, P.V., Kamath, R.S., Fraser, A.G., Ahringer, J. and Plasterk, R.H. (2003) Genome-wide RNAi of *C. elegans* using the hypersensitive *rrf-3* strain reveals novel gene functions. PLoS Biol. **1**, E12 CrossRef PubMed

68 Sönnichsen, B., Koski, L.B., Walsh, A., Marschall, P., Neumann, B., Brehm, M., Alleaume, A.M., Artelt, J., Bettencourt, P., Cassin, E. et al. (2005) Full-genome RNAi profiling of early embryogenesis in *Caenorhabditis elegans*. Nature **434**, 462–469 CrossRef PubMed

69 Ceron, J., Rual, J.F., Chandra, A., Dupuy, D., Vidal, M. and van den Heuvel, S. (2007) Large-scale RNAi screens identify novel genes that interact with the *C. elegans* retinoblastoma pathway as well as splicing-related components with synMuv B activity. BMC Dev. Biol. **7**, 30 CrossRef PubMed

70 Gravato-Nobre, M.J., Nicholas, H.R., Nijland, R., O'Rourke, D., Whittington, D.E., Yook, K.J. and Hodgkin, J. (2005) Multiple genes affect sensitivity of *Caenorhabditis elegans* to the bacterial pathogen *Microbacterium nematophilum*. Genetics **171**, 1033–1045 PubMed

Received 1 July 2015/13 March 2016; accepted 23 March 2016
Accepted Manuscript online 23 March 2016, doi:10.1042/BCJ20160142